Chapter 6. Trends in IMPROVE Speciated Aerosol Concentrations

Site-specific trends were computed for eight parameters: 10th, 50th, and 90th percentiles and winter (DJF), spring (MAM), summer (JJA), fall (SON), and annual mean. December data from the previous year were included in winter mean calculations. Fifty percent of daily data was required for a valid seasonal mean, and annual means were calculated from four valid seasonal means. Annual percentiles were calculated for 60% of valid daily data. Long- and short-term trends required 70% of the years to be valid. These completeness criteria differed from those applied for 4-year aggregated data (see Chapter 2). A Theil regression was performed with the concentration data as the dependent variable and the year as the independent variable. Theil regressions avoid heavy influence by outliers on the regression results (Theil, 1950). Kendall tau statistics were used to determine the statistical significance, assuming the slope was statistically significant at 5% ($p \leq 0.05$), meaning that there was a 95% chance that the slope was not due to random chance. Trends (% yr^{-1}) were calculated by dividing the slope by the median concentration value over the time period of the trend, multiplied by 100%. Reporting trends instead of slopes normalizes the range in concentrations that occur across the United States. However, trends can be large when median concentrations are very low (e.g., 10th percentile).

Short-term, regional mean trends were calculated for ten regions of the United States. Sites were grouped by their state into the following regions: Northeast, Southeast, Midsouth, Central, Southwest, Northwest, California, Alaska, Hawaii, Virgin Islands (see Table 6.0 and Figure 6.0) and the continental United States (CONUS). The Virgin Islands region included one site. Although some names are the same, these regions are broader and do not necessarily correspond to the regions shown in Chapters 3 and 5. The regions were qualitatively determined only as a means for summarizing trends. Regional mean trends were computed by aggregating site-specific seasonal mean concentrations (or percentiles) for a given region and year and then performing a Theil regression on regional mean concentrations. Sites that met the 70% valid data trend requirement were included in the regional trend calculation. Regional mean trends were calculated for seasonal and annual means and for the 10th, 50th, and 90th percentiles. Annual mean trends can be driven by specific seasons, and different parts of the mass distribution may have different trends, so comparisons of regional mean trends provide further insight into temporal behavior of major aerosol components.

Table 6.0. Regions and states (abbreviations) used for regional mean trends. Sites within listed states were included in the corresponding region.

Region	State
Northeast	ME, NH, VT, MA, RI, CT, NY, PA, NJ, DE, MD, OH, WV, VA, IN, KY
Southeast	TN, NC, SC, MS, LA, AL, GA, FL
Midsouth	OK, LA, AR
Central	ND, SD, MN, MI, WI, IL, MO, KS, NE, IA
Southwest	NV, UT, CO, NM, AZ, TX
Northwest	WA, OR, ID, MT, WY
California	CA
Alaska	AK
Hawaii	HI
Virgin Islands	Virgin Islands

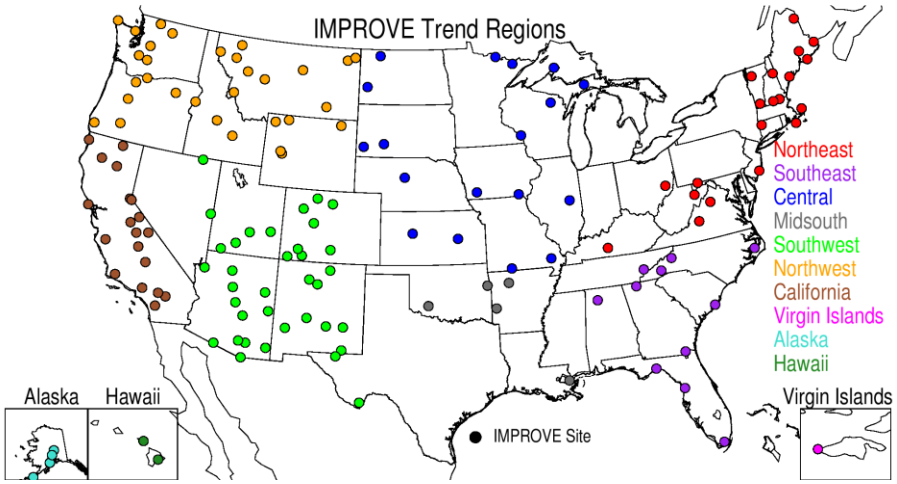

Figure 6.0. IMPROVE regions defined to summarize regional mean trends.

Trend results were interpolated to provide isopleths to guide the eye (Isaaks and Mohan Srivastava, 1989). Positive trends are denoted with an upward-pointing triangle and contoured with warm colors. Negative trends are shown with downward-pointing triangles and contoured with cold colors. Statistically significant trends ($p \leq 0.05$) are denoted with filled triangles. Scales were kept similar for all parameters so that trends can be compared. Long-term trend maps suffer from lower site densities, and therefore interpolations in regions without long-term sites (such as the central United States) should be viewed only as a spatial transition.

6.1 SULFATE ION TRENDS

Missing sulfate ion concentrations after 1 May 1995 were replaced with 3 × sulfur concentrations to reduce the impacts of missing data on trend results. Before 1995, filters were masked and could result in an underestimation of sulfur concentrations (Schichtel, 2003); therefore sulfur was not used as a replacement before this date. Long-and short-term annual mean sulfate ion trends are shown in Figures 6.1.1a and 6.1.1b, respectively. Fifty-five sites met long-term annual mean trend completeness criteria, and most long-term sites are in the western United States. Annual mean sulfate ion concentrations have decreased significantly for all CONUS long-term sites. Long-term annual mean sulfate ion trends ranged from -7.78% yr^{-1} ($p < 0.001$) at Shining Rock Wilderness Area (WA), North Carolina (SHRO1), to -1.01% yr^{-1} ($p = 0.01$) at Lassen Volcanic National Park (NP), California (LAVO1). The greatest long-term decrease in annual mean sulfate ion concentrations occurred for sites along the Appalachian region where sulfur dioxide emissions have also dramatically decreased (Krotkov et al., 2016; Kharol et al., 2017; Feng et al., 2020; Hand et al., 2020). Less progress occurred for sites in California, Nevada, and Idaho, as well as southwestern Texas. Trends at these sites were between -1% yr^{-1} and -2% yr^{-1}. Emissions in the West have historically been lower than in the East (Hand et al., 2012; Hand et al., 2020), and therefore the reduction of those regulated emissions has had less of an impact on already-low concentrations.

(a)

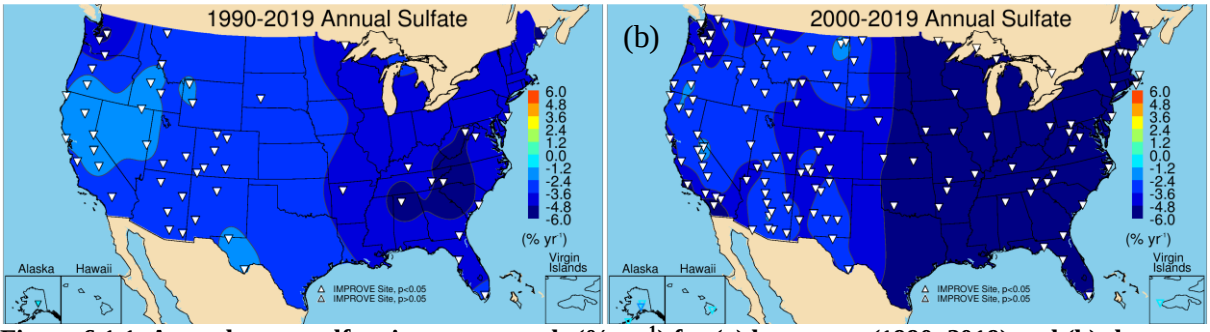

Figure 6.1.1. Annual mean sulfate ion mass trends (% yr^{-1}) for (a) long-term (1990–2019) and (b) short-term (2000-2019) periods. Filled triangles correspond to statistically significant trends ($p \leq 0.05$).

Annual mean sulfate ion concentrations also decreased for all of the short-term sites shown in Figure 6.1.1b. Out of the 135 valid sites, all but five had statistically significant annual mean sulfate ion trends that ranged from -11.23% yr^{-1} ($p < 0.001$) at Cohutta, Georgia (COHU1), to -1.76% yr^{-1} ($p = 0.012$) at Fort Peck, Montana (FOPE1). Insignificant trends occurred at sites in Hawaii, Alaska, and the Virgin Islands. As seen in Figure 6.1.1b, a strong spatial gradient in annual mean trends existed between the eastern and western United States, with stronger rates of change for sites in the East. Sites east of -100° nearly all had concentrations decrease at rates greater than -4% yr^{-1}, and at sites in the Appalachia and Ohio River valley regions, trends were around -7% yr^{-1} to -10% yr^{-1}, corresponding to a 140–200% decrease over the past two decades. Trends at sites in the western United States were about -2% yr^{-1} to -4% yr^{-1}.

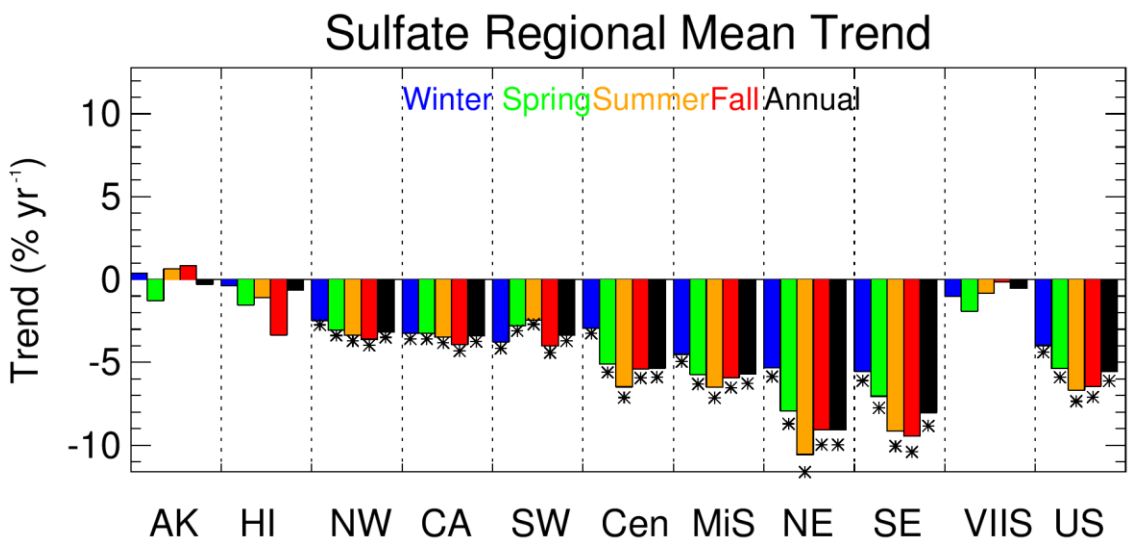

Figure 6.1.2. Short-term (2000–2019) regional seasonal mean sulfate ion trends (% yr^{-1}) for major U.S. regions for winter, spring, summer, fall, and annual means. Regions are arranged from western to eastern United States (AK = Alaska, HI = Hawaii, NW = Northwest, CA= California, SW = Southwest, Cen = Central, MiS = Midsouth, NE = Northeast, SE = Southeast, VIIS = Virgin Islands, and US = all sites). Statistically significant trends ($p \leq 0.05$) are denoted with "*".

The spatial gradients and seasonal distribution in sulfate ion trends are also shown in the regional mean trends presented in Figure 6.1.2, with regional mean trends ordered from west to

east. The largest reductions in seasonal mean sulfate ion concentrations occurred for sites in the Northeast region (-10.56% yr^{-1} in summer), followed by the Southeast region (-9.46% yr^{-1} in fall). For the Northeast, Midsouth, and Central regions, the largest decrease in sulfate ion concentrations occurred during summer (in the Southeast decreases in fall were slightly larger), and the lowest decreases occurred during winter. This difference in the seasonal mean trends has led to a decrease in the seasonality of sulfate ion concentrations at eastern regions, as was discussed in Chapter 3. In regions in the western United States, the rate of decrease was lower, roughly half of the rate of decrease relative to eastern regions. The differences in seasonal mean trends were also smaller, suggesting that sulfate ion concentrations decreased by similar rates across seasons. The exception to this is at the Southwest region, where the largest decreases occurred during both winter and fall. Overall, across the United States, sulfate ion concentrations have decreased at a higher rate during summer and fall. Seasonal mean trends at sites in Alaska, Hawaii, and the Virgin Islands were all relatively flat and insignificant.

Long-term 10th and 90th percentile sulfate ion trends are shown in Figure 6.1.3a and 6.1.3b, respectively. The 50th percentile trends are not shown, as they are similar to the annual mean trends previously discussed. The spatial variability for the 10th and 90th percentile trends were similar, with larger reductions in the eastern United States. The 10th percentile trends ranged from -6.01% yr^{-1} ($p < 0.001$) at Snoqualmie Pass, Washington (SNPA1), to -1.13% yr^{-1} ($p = 0.04$) at Yosemite NP, California (YOSE1), and 54 out of 57 sites had statistically significant trends. Insignificant trends occurred at Hawaii Volcanoes NP, Hawaii (HAVO1), Lassen Volcanic NP, California (LAVO1), and Three Sisters WA, Oregon (THSI1). Trends in the 10th percentile sulfate ion concentrations at sites in California were weaker (~ -2% yr^{-1}) than for other areas in the United States.

Trend values did not differ greatly for the long-term 90th percentile in sulfate concentrations (Figure 6.1.3b) compared to the 10th percentile trends, and 55 out of 57 sites had statistically significant trends. The largest negative trend occurred at Shining Rock WA, North Carolina (SHRO1, -7.31% yr^{-1}, $p < 0.001$) compared to the least negative trend at Big Bend NP, Texas, (BIBE1, -0.81% yr^{-1}, $p = 0.03$). Trends for sites in Arizona and New Mexico were somewhat larger for the 90th percentile compared to the 10th percentile, while trends at sites in California were similar. Greater reductions in the 90th percentile concentration trends (-5% yr^{-1}) occurred at sites in the East.

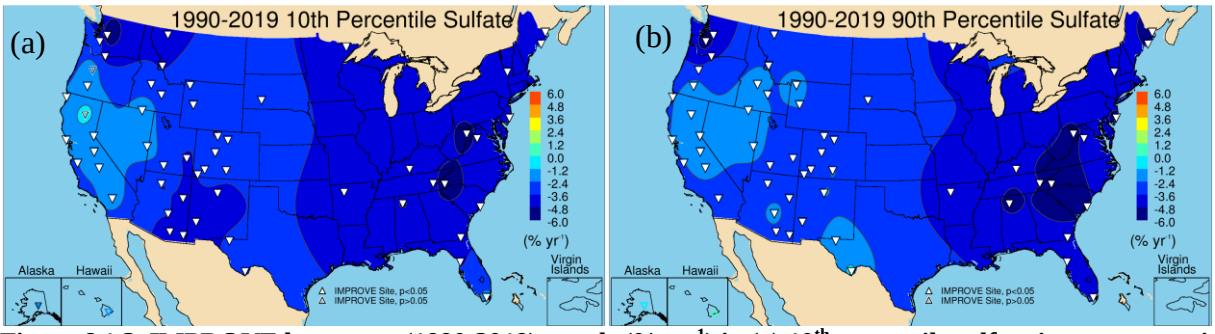

Figure 6.1.3. IMPROVE long-term (1990-2019) trends (% yr^{-1}) in (a) 10th percentile sulfate ion concentrations and (b) 90th percentile concentrations. Filled triangles correspond to statistically significant trends ($p \leq 0.05$).

Short-term trends in the 10th and 90th percentile sulfate ion concentrations are shown in Figure 6.1.4a and 6.1.4b, respectively. Large-scale spatial variability in trends was similar for both percentiles, with greater reductions in sulfate ion concentrations at sites in the eastern United States. Differences in the spatial patterns occurred in the central United States and for some sites in California that experienced insignificant 10th percentile trends. For 138 sites with valid 10th percentile trends, 126 were statistically significant, compared to 132 for 90th percentile trends. The largest reduction in 10th percentile concentrations occurred at Cohutta, Georgia (COHU1, -8.30% yr^{-1}, $p < 0.001$), compared to the least reduction at Bliss State Park (SP), California (BLIS1, -1.73% yr^{-1}, $p = 0.03$). The largest reduction in the 90th percentile concentrations also occurred at Cohutta, Georgia (COHU1, -14.22% yr^{-1}, $p < 0.001$), compared to Kaiser, California (KAIS1, -1.40% yr^{-1}, $p = 0.03$). For both the 10th and 90th percentiles, trends were negative but insignificant at Alaska, Hawaii, and Virgin Island sites.

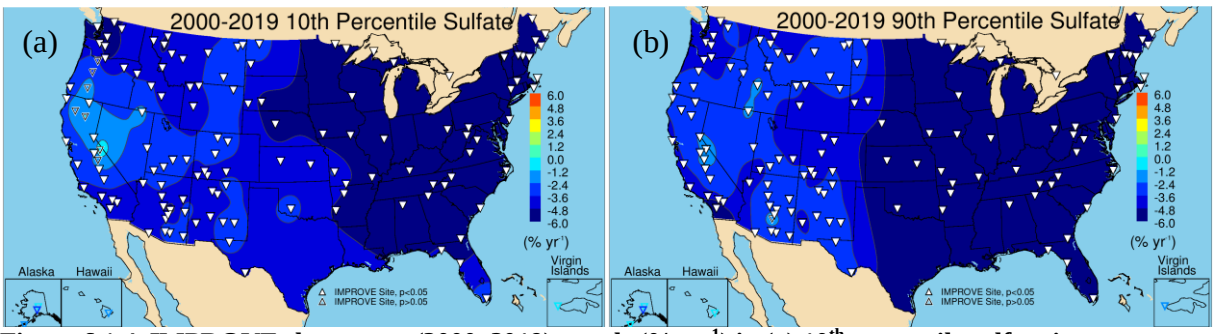

Figure 6.1.4. IMPROVE short-term (2000–2019) trends (% yr^{-1}) in (a) 10th percentile sulfate ion concentrations and (b) 90th percentile concentrations. Filled triangles correspond to statistically significant trends ($p \leq 0.05$).

Comparisons of short-term regional mean percentile trends are shown in Figure 6.1.5. For most regions in the western United States, the 10th, 50th, and 90th percentiles were similar, with the Northwest and Southwest regions having slightly greater reductions in the 10th percentile concentrations and the California region having somewhat greater reductions in the regional mean 90th percentile concentrations. However, for eastern regions, the regional 90th percentile trends decreased at a much greater rate than the 10th and 50th percentile concentrations. The Northeast region 90th percentile trend was -10.51% yr^{-1} ($p < 0.001$) compared to the 10th percentile trend of -6.46% yr^{-1} ($p < 0.001$). The Southeast region had a similar difference in 90th and 10th percentile trends (-9.63% yr^{-1}, $p < 0.001$, compared to -5.28% yr^{-1}, $p < 0.001$, respectively). These trends are consistent with the seasonal mean trends, as the highest sulfate ion concentrations typically occurred during summer.

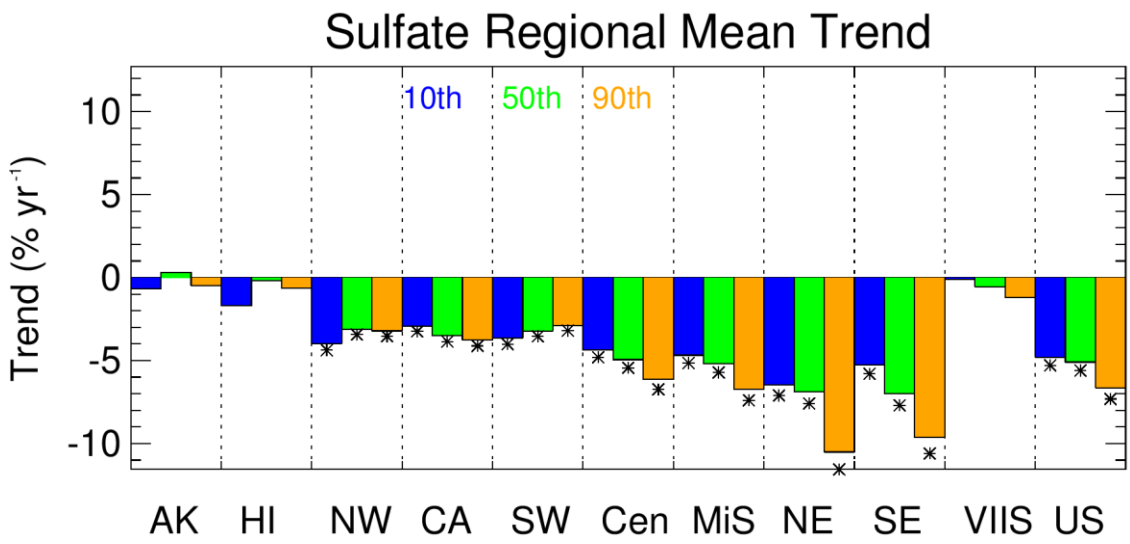

Figure 6.1.5. Short-term (2000–2019) regional mean trends (% yr^{-1}) in 10th, 50th, and 90th percentile sulfate ion concentrations. Regions are arranged from western to eastern United States (AK = Alaska, HI = Hawaii, NW = Northwest, CA= California, SW = Southwest, Cen = Central, MiS = Midsouth, NE = Northeast, SE = Southeast, VIIS = Virgin Islands, and US = all sites). Statistically significant trends ($p \leq 0.05$) are denoted with "*".

6.2 NITRATE ION TRENDS

During the late 1990s, IMPROVE nitrate ion concentrations at many sites fell below historical values during winter months. Investigations into the period from 1996 through 2000 revealed lower than usual concentrations during winter months, and the cause remains unknown (McDade, 2004; McDade, 2007). Concentrations returned to normal levels after 2000, after which the data were deemed valid. Given the number of sites influenced by this anomaly (Debell, 2006), nitrate ion data were considered invalid for winters from 1996 through 2000, which invalidated annual mean and percentile concentrations for those years.

Long-term annual mean nitrate ion trends are shown in Figure 6.2.1a. Of the 42 valid trend sites, 36 had statistically significant trends. The largest reductions in the annual mean nitrate ion concentrations occurred at sites in southern California and were about -3% yr^{-1}, except at the site with the largest negative trend, San Gorgonio WA, California (SAGO1, -7.95% yr^{-1}, $p < 0.001$). Strong reductions in nitrate ion concentrations in California are associated with reduced nitrogen dioxide emissions from vehicles (Krotkov et al., 2016; Hand et al., 2020). Insignificant trends occurred at sites in the southwestern United States and were associated with nearly flat reductions. The lowest statistically significant trend occurred at Bridger WA, Wyoming (BRID1, -0.92% yr^{-1}, $p = 0.04$). Sites in the eastern United States corresponded to reductions about -1% yr^{-1} to -2% yr^{-1}.

Short-term annual mean nitrate trends also showed strong reductions at sites in southern California (Figure 6.2.1b). The strongest reductions for short-term trends occurred at San Gorgonio, California (SAGO1, -8.89% yr^{-1}, $p < 0.001$). Around 80% of short-term annual mean nitrate trends were statistically significant (109 out of 134 valid sites). Sites in the northern Great

Plains were associated with insignificant trends (-1% yr^{-1} to -2% yr^{-1}), likely due to the influence of oil and gas development in the region (Prenni et al., 2016; Evanoski-Cole et al., 2017; Gebhart et al., 2018). The lowest statistically significant annual mean nitrate ion trend occurred at Swanquarter, North Carolina (SWAN1, -0.88% yr^{-1}, $p = 0.04$).

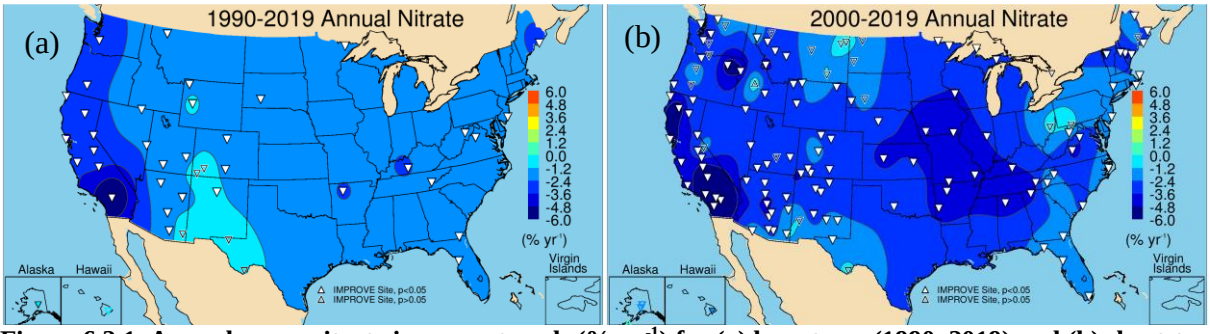

Figure 6.2.1. Annual mean nitrate ion mass trends (% yr^{-1}) for (a) long-term (1990–2019) and (b) short-term (2000–2019) periods. Filled triangles correspond to statistically significant trends ($p \leq 0.05$).

Comparisons of short-term regional seasonal mean nitrate ion concentration trends are shown in Figure 6.2.2. As seen in Figure 6.2.1b, the strongest reductions occurred in the California region, especially in fall (-7.46% yr^{-1}, $p < 0.001$) and spring (-7.00% yr^{-1}, $p < 0.001$). In other regions, there were differences in seasonal mean trends. For example, the regions of the Northwest, Southwest, and Southeast followed a similar pattern, with winter trends having the largest reductions, compared to the lowest reductions in summer, and spring and fall were in-between and comparable. This pattern is different from what occurred in the Midsouth region, with the strongest trends in spring, and the Central region, where the fall trends were the strongest and summer trends were lowest and insignificant. In contrast, very little range in seasonal trends occurred in the Northeast region (and winter had the lowest reductions). This range in seasonal mean trends indicates potentially different sources and atmospheric processes controlling nitrate concentrations in these regions.

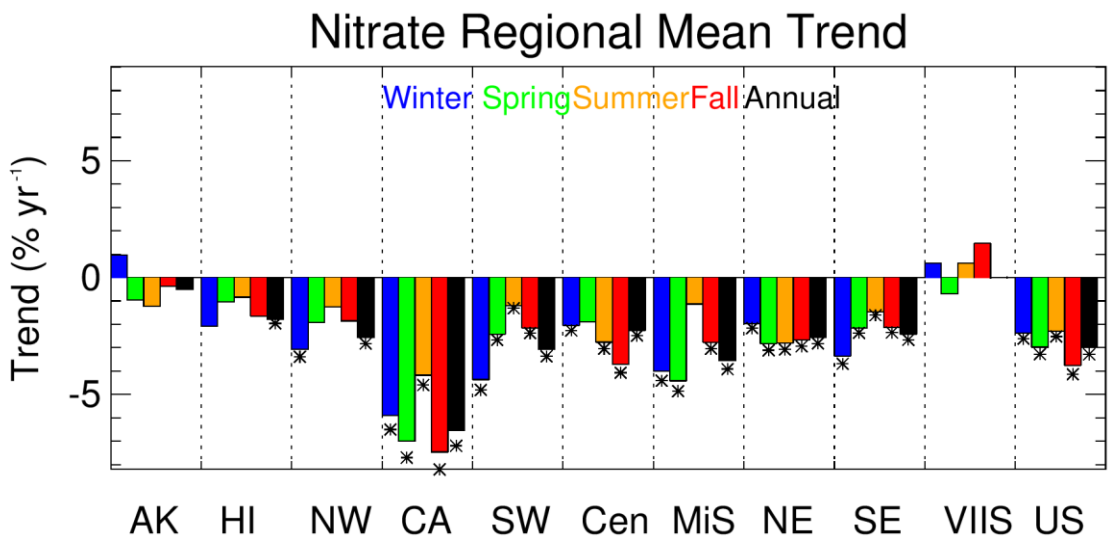

Figure 6.2.2. Short-term (2000–2019) regional seasonal mean nitrate ion trends (% yr^{-1}) for major U.S. regions for winter, spring, summer, fall, and annual means. Regions are arranged from western to eastern United States (AK = Alaska, HI = Hawaii, NW = Northwest, CA= California, SW = Southwest, Cen = Central, MiS = Midsouth, NE = Northeast, SE = Southeast, VIIS = Virgin Islands, and US = all sites). Statistically significant trends ($p \leq 0.05$) are denoted with "*".

Long-term trends in the 10th and 90th percentile nitrate concentrations are shown in Figure 6.2.3a and 6.2.3b, respectively. Of the 45 valid sites, only 25 of them were associated with statistically significant trends, and these occurred mainly at sites in California and the eastern United States. Similar to the annual mean trend, the strongest reduction in the 10th percentile nitrate concentration occurred at San Gorgonio WA, California (SAGO1, -6.03% yr^{-1}, $p < 0.001$), compared to -1.00% yr^{-1} ($p = 0.02$) at Great Sand Dunes NP, Colorado (GRSA1). Many of the sites associated with insignificant and flat trends were located in the southwestern United States and the Intermountain West.

The spatial patterns in the 10th and 90th percentile long-term trends were similar, with the strongest reductions at sites in California, and weak and insignificant trends at sites in the Southwest. However, more sites met statistical significance criteria (30 out of 45) for 90th percentile trends. Some long-term trends at sites in the eastern United States were not as strong for the 90th percentile relative to the 10th percentile concentrations, and some 90th percentile trends were insignificant while the 10th percentile trends were not (Great Smoky Mountains NP, Tennessee, GRSM1 and Mammoth Cave NP, Kentucky, MACA1).

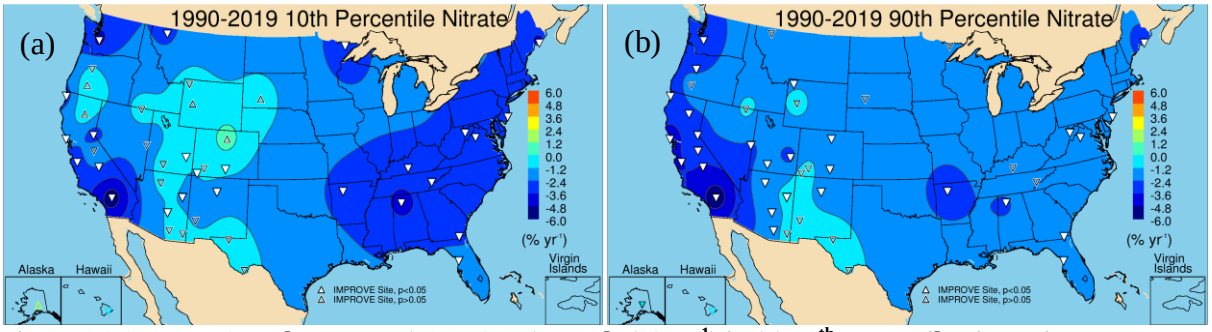

Figure 6.2.3. IMPROVE long-term (1990–2019) trends (% yr^{-1}) in (a) 10th percentile nitrate ion concentrations and (b) 90th percentile concentrations. Filled triangles correspond to statistically significant trends ($p \leq 0.05$).

The strongest reductions in short-term 10th percentile nitrate concentration trends also occurred at San Gorgonio WA, California (SAGO1, -10.34% yr^{-1}, $p < 0.001$) (Figure 6.2.4a). Several sites in the eastern United States also experienced strong reductions in the 10th percentile concentrations (-5% yr^{-1} to -6% yr^{-1}), such as Cohutta, Georgia (COHU1); Seney, Michigan (SENE1); James River Face WA, Virginia (JARI1); and Quabbin Summit, Massachusetts (QURE1). Insignificant trends occurred at 81 of 138 valid sites. Positive but insignificant trends occurred at sites in the northern Great Plains, where oil and gas development has influenced nitrate concentrations. Other insignificant trends occurred at sites in Wyoming, Colorado, and Texas. The weakest significant trend occurred at Wichita Mountains, Oklahoma (WIMO1, -1.34% yr^{-1}, $p = 0.04$).

The spatial pattern in the short-term 90th percentile trend (Figure 6.2.4b) was similar to the 10th percentile trend pattern, with the strongest negative trends at sites in southern California, and at sites in Appalachian Mountains. Out of 138 valid sites, 98 met statistical significance requirements. Most of the insignificant trends also occurred at sites in the northern Great Plains area and near Maryland and Ohio (Frostburg Reservoir, Maryland, FRRE1, and Quaker City, Ohio, QUCI1, respectively).

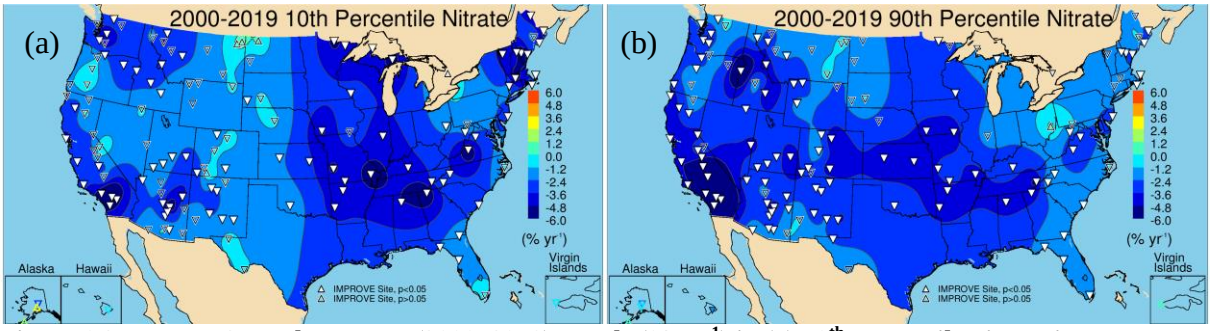

Figure 6.2.4. IMPROVE short-term (2000–2019) trends (% yr^{-1}) in (a) 10th percentile nitrate ion concentrations and (b) 90th percentile concentrations. Filled triangles correspond to statistically significant trends ($p \leq 0.05$).

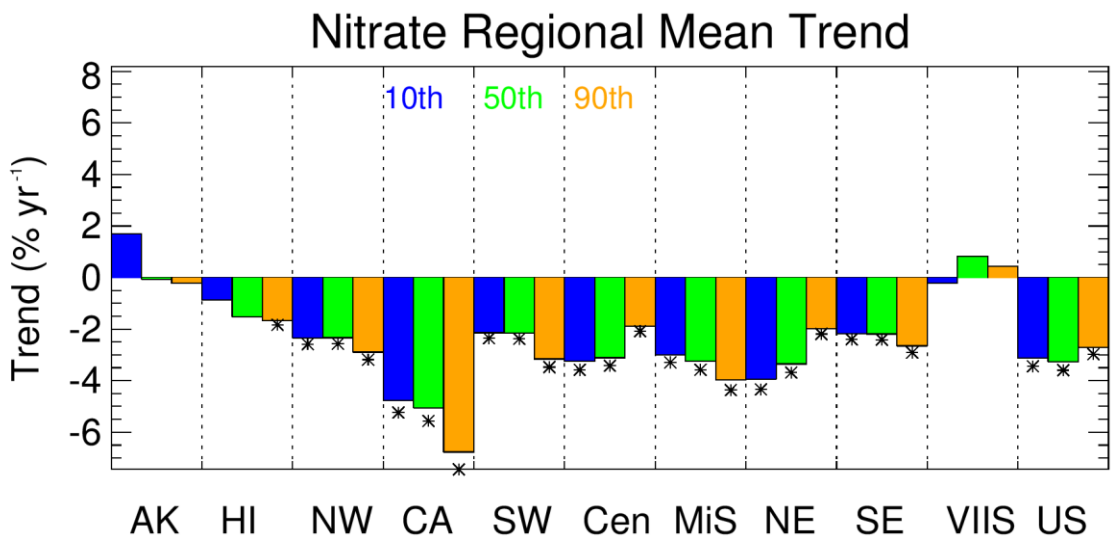

Figure 6.2.5. Short-term (2000–2019) regional mean trends (% yr^{-1}) in 10th, 50th, and 90th percentile nitrate ion concentrations. Regions are arranged from western to eastern United States (AK = Alaska, HI = Hawaii, NW = Northwest, CA= California, SW = Southwest, Cen = Central, MiS = Midsouth, NE = Northeast, SE = Southeast, VIIS = Virgin Islands, and US = all sites). Statistically significant trends ($p \leq 0.05$) are denoted with "*".

A summary of the regional 10th, 50th, and 90th percentile nitrate ion concentration trends is shown in Figure 6.2.5. As was seen in the maps, the strongest trends occurred in the California region, with the 90th percentile trends being the greatest (-6.77% yr^{-1}, $p < 0.001$). For all of the regions, except the Central and Northeast regions, reductions in the 90th percentile concentrations were strongest. In the Central and Northeast regions, the 90th percentile trends were the weakest, and the 10th percentile trends were the strongest. Reasons for this pattern for these regions is unknown.

6.3 ORGANIC CARBON TRENDS

Trends in OC and EC may be affected by changes in analytical methods. A recent review of carbonaceous measurements in the IMPROVE program identified shifts in analytical methods and their impacts on the fraction of EC to total carbon (OC + EC), i.e., EC/TC (Schichtel et al., 2021). One such shift occurred with hardware upgrades in 2005 that resulted in changes in the split between OC and EC that introduced uncertainty to trend analyses (Chow et al., 2007; White, 2007). Other shifts in EC/TC have also occurred over the history of the program due to new analyzers, new calibrations, and undetermined reasons. These effects have motivated discussions regarding future carbonaceous aerosol measurements within the program (Schichtel et al., 2021).

Annual mean OC trends for long-term sites are shown in Figure 6.3.1a. Of the 51 valid sites, 32 had statistically significant trends, including all of the sites in the eastern United States. Insignificant trends occurred at sites in the Intermountain West and at sites along eastern California. Positive but insignificant trends occurred at Bridger WA, Wyoming (BRID1); Crater Lake NP, Oregon (CRLA1); and Lassen Volcanic NP, California (LAVO1), sites likely

associated with impacts from biomass burning. The strongest statistically significant reductions in OC occurred at Mount Rainier NP, Washington (MORA1, -3.36% yr^{-1}, $p < 0.001$), and the least reduction occurred at Guadalupe Mountains, NP, Texas (GUMO1, -1.06% yr^{-1}, $p = 0.009$). Other strong reductions in the West occurred at Point Reyes National Seashore, California (PORE1, -3.24% yr^{-1}, $p < 0.001$), and San Gorgonio WA, California (SAGO1, -2.97% yr^{-1}, $p < 0.001$). Strong reductions in the East occurred at Dolly Sods WA, West Virginia (DOSO1, -2.93% yr^{-1}, $p < 0.001$); Shenandoah NP, Virginia (SHEN1, -2.44% yr^{-1}, $p < 0.001$); and Moosehorn National Wildlife Refuge (NWR), Maine, (MOOS1, -2.98% yr^{-1}, $p < 0.001$). Reductions in anthropogenic emissions have led to a decrease in OC in the East (e.g., Blanchard et al., 2016; Malm et al., 2017).

With the addition of short-term sites, the area with insignificant short-term trends increased farther north (Figure 6.3.1b), at sites in Montana, Idaho, and Washington, where biomass smoke has influenced trends in particulate matter and OC (McClure and Jaffe, 2018). All of the sites with insignificant trends occurred in the western United States and in Alaska, Hawaii, and the Virgin Islands. Positive, but insignificant, trends occurred at Craters of the Moon National Monument (NM), Idaho (CRMO1); White Pass, Washington (WHPA1); and Hoover, California (HOOV1), among others. Of the 136 valid sites, 67 had statistically significant trends. The strongest reduction occurred at Agua Tibia, California (AGTI1, -4.25% yr^{-1}, $p < 0.001$), and the least reduction occurred at Isle Royale NP, Michigan (ISLE1, -1.39% yr^{-1}, $p = 0.003$). Relatively strong reductions in annual mean OC occurred at sites in the eastern and northeastern United States. In the western United States, strong reductions also occurred at sites in southern California and parts of Arizona and New Mexico.

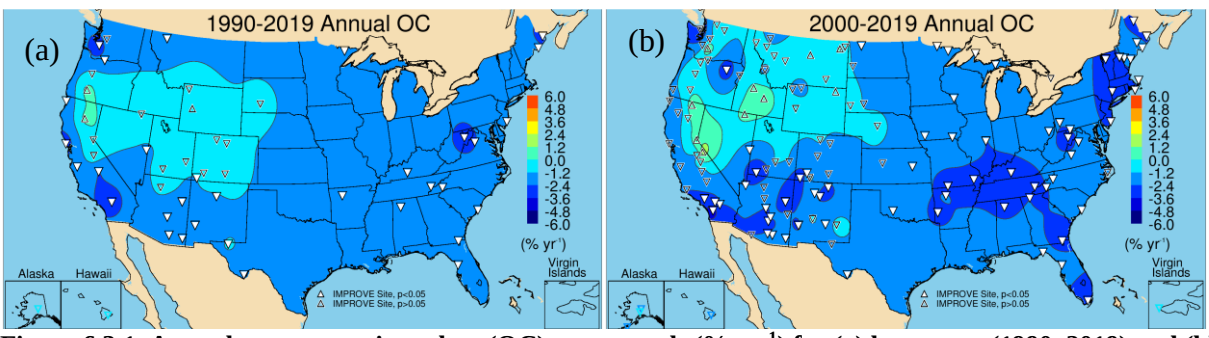

Figure 6.3.1. Annual mean organic carbon (OC) mass trends (% yr^{-1}) for (a) long-term (1990–2019) and (b) short-term (2000–2019) periods. Filled triangles correspond to statistically significant trends ($p \leq 0.05$).

Regional seasonal mean OC trends are shown in Figure 6.3.2. Statistically significant trends occurred during all seasons in the Southeast, Northeast, and the Midsouth regions, about -3% yr^{-1}. The strongest reductions in most these regions occurred for winter and spring. Trends in the Central region were lower (~-2% yr^{-1}) than regions in the East and statistically significant in all seasons except summer. Seasonal mean trends at western regions were more variable than in the East. All of the winter and spring trends were statistically significant, and OC declined more strongly in these months (-3% yr^{-1} to -4% yr^{-1}). Summer and fall trends were insignificant and summer trends were flat in the Northwest and California regions. Trends during these seasons have been influenced by biomass burning emissions.

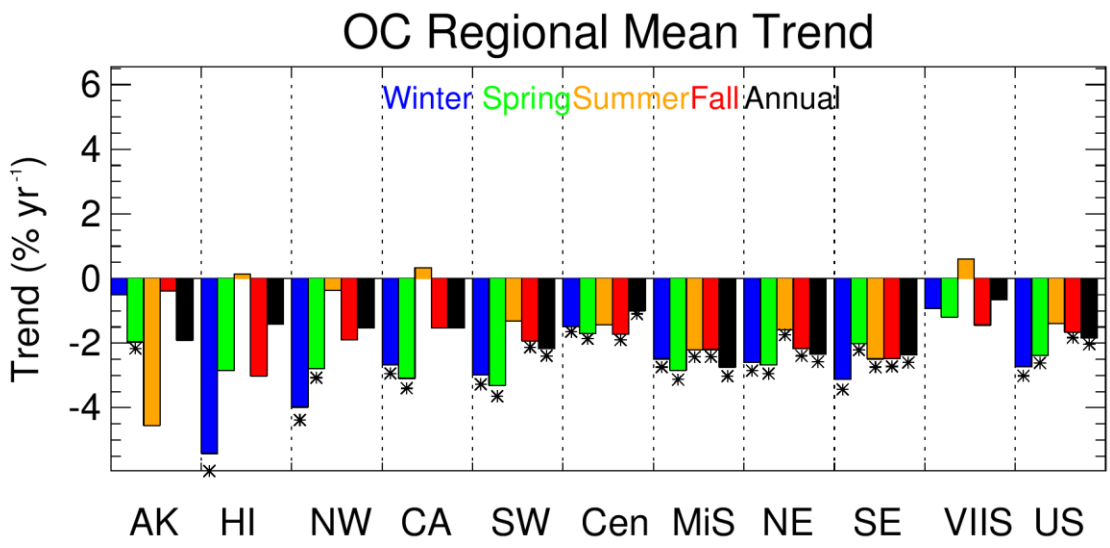

Figure 6.3.2. Short-term (2000–2019) regional seasonal mean organic carbon (OC) trends (% yr^{-1}) for major U.S. regions for winter, spring, summer, fall, and annual means. Regions are arranged from western to eastern United States (AK = Alaska, HI = Hawaii, NW = Northwest, CA= California, SW = Southwest, Cen = Central, MiS = Midsouth, NE = Northeast, SE = Southeast, VIIS = Virgin Islands, and US = all sites). Statistically significant trends ($p \leq 0.05$) are denoted with "*".

Differences in spatial patterns for long-term trends in the 10th and 90th percentile OC concentrations were evident from comparing Figure 6.3.3a and 6.3.3b, respectively. Reductions in the 10th percentile OC concentrations were much greater than for the 90th percentile concentrations, especially for sites in the West. Of the 51 long-term valid sites, 49 had statistically significant trends in 10th percentile OC concentrations. Strong reductions occurred at sites in northern California, Oregon, and Washington (-5% yr^{-1} to -6% yr^{-1}), with the strongest at Mount Rainier NP, Washington (MORA1, -7.07% yr^{-1}, $p < 0.001$). However, sites across the United States experienced reductions around -2% yr^{-1} or greater. The lowest reduction occurred at Great Sand Dunes NP, Colorado (GRSA1, -1.01% yr^{-1}, $p = 0.02$). In contrast, 90th percentile trends at sites across the western United States were mostly insignificant, with over half (26) of the sites not meeting the statistical significance criterion. Ten of these sites were associated with positive but insignificant trends. These results suggest different influences on trends for different parts of the OC mass distribution. The trends in the highest OC concentrations were likely influenced by biomass burning impacts.

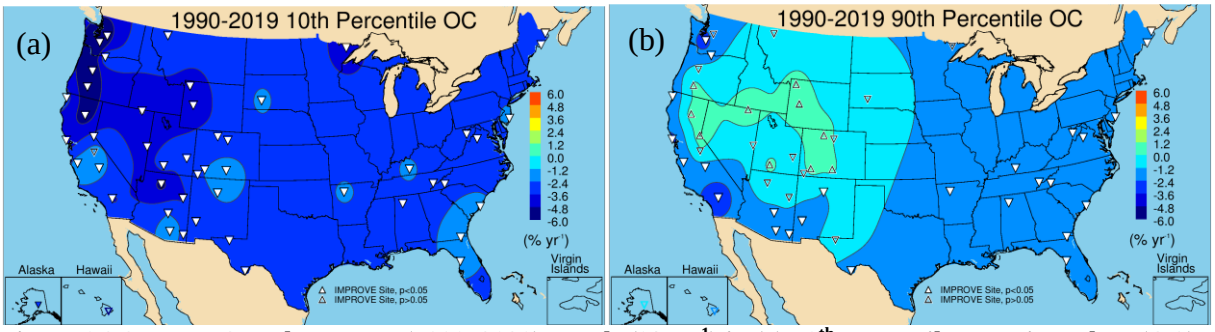

Figure 6.3.3. IMPROVE long-term (1990–2020) trends (% yr^{-1}) in (a) 10th percentile organic carbon (OC) concentrations and (b) 90th percentile concentrations. Filled triangles correspond to statistically significant trends ($p \leq 0.05$).

A similar spatial pattern occurred for short-term 10th and 90th percentile OC trends (Figure 6.3.4a and 6.3.4b, respectively). Most of the 10th percentile trends were statistically significant (90 out of 138 valid sites), and nearly all of these sites were in the eastern United States. Many of the trends at sites in the West were negative and insignificant, except for five sites. The greatest reductions occurred at North Absaroka, Wyoming (NOAB1, -11.68% yr^{-1}, p = 0.009), compared to the positive trend at Virgin Islands NP (VIIS1, 12.76% yr^{-1}, p = 0.011). The strongly positive trend at VIIS1 is likely due to very low 10th percentile OC concentrations. Recall that trends were calculated by dividing the slope from the regression by the median of the concentration over the period, so sites with very low 10th percentile concentrations may have elevated trends.

While most of the sites in the eastern United States had statistically significant short-term 90th percentile trends, many of the sites in the West did not (51 out of 138 valid sites). Many of these same insignificant trend sites also had insignificant trends in annual mean OC; however, these sites did not have insignificant 10th percentile trends. It appears that the influences on the high OC concentrations were not similarly affecting the lowest OC concentrations over time. The strongest reductions in the 90th percentile trends occurred at Starkey, Oregon (STAR1, -4.22% yr^{-1}, p = 0.03), compared to -1.54% yr^{-1} (p = 0.003) at Quaker City, Ohio (QUCI1).

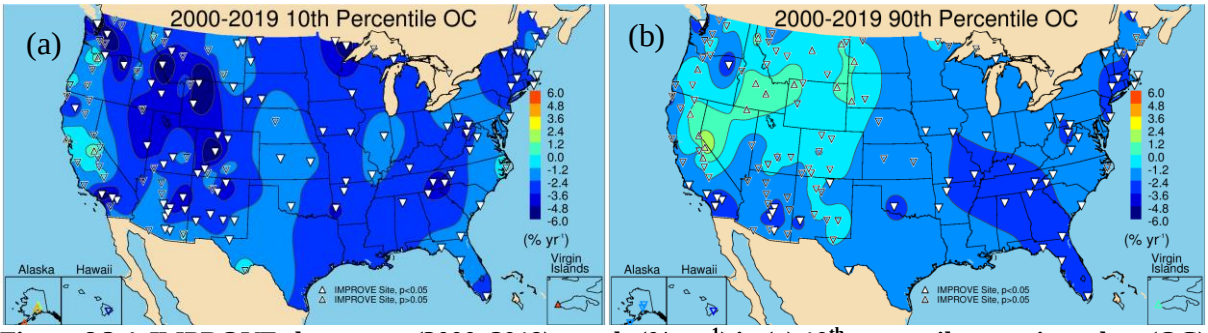

Figure 6.3.4. IMPROVE short-term (2000–2019) trends (% yr^{-1}) in (a) 10th percentile organic carbon (OC) concentrations and (b) 90th percentile concentrations. Filled triangles correspond to statistically significant trends ($p \leq 0.05$).

Differences in the trends in the 10th and 90th percentiles are shown in the regional mean percentile trends in Figure 6.3.5. The 90th percentile trends were the weakest and statistically

insignificant for regions in the West, such as the Northwest, California, and the Southwest regions. For regions in the East, the trends were similar for the lowest and highest OC concentrations, and all were statistically significant, indicating different influences on OC trends in the eastern and western United States, especially for the highest OC concentration in the West. Very large 10th percentile trends in the Virgin Islands and Hawaii regions were likely due to very low normalizing concentrations.

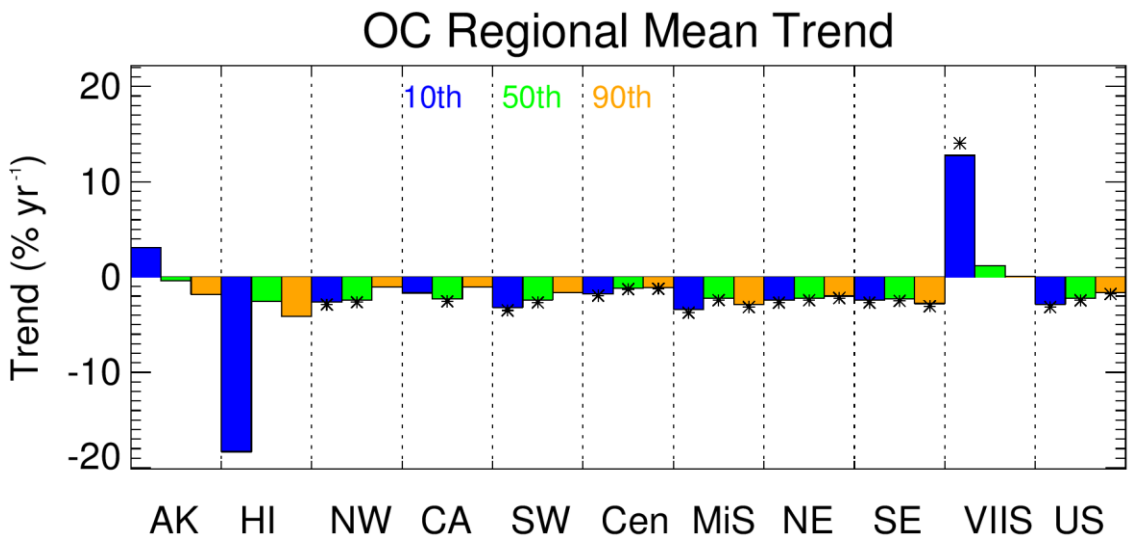

Figure 6.3.5. Short-term (2000-2019) regional mean trends (% yr^{-1}) in 10th, 50th, and 90th percentile organic carbon (OC) concentrations. Regions are arranged from western to eastern United States (AK = Alaska, HI = Hawaii, NW = Northwest, CA= California, SW = Southwest, Cen = Central, MiS = Midsouth, NE = Northeast, SE = Southeast, VIIS = Virgin Islands, and US = all sites). Statistically significant trends ($p \leq 0.05$) are denoted with "*".

6.4 ELEMENTAL CARBON TRENDS

EC trends are affected by hardware and analytic changes, similar to issues that affect OC trends, as discussed in Section 6.3. In addition, Malm et al. (2020) suggested EC may be inadvertently and incorrectly assigned to the OC fraction during the thermal optical reflectance analysis, resulting in an underestimate of true EC concentrations. As discussed by Schichtel et al. (2021), EC concentrations have decreased at rural sites to the point that many sites have concentrations that are below the lower quantifiable limits (LQL, defined as 3 × minimum detection limit, MDL). From 2017 to 2019, about 30% of all EC concentrations were below the LQL. More sites in the West were below LQL than in the East. These low concentrations make tracking trends difficult, especially for the 10th percentile concentrations.

Long-term trends in annual mean EC are shown in Figure 6.4.1a. Of the 51 valid sites, 48 had statistically significant negative trends. The strongest reduction occurred at Hawaii Volcanoes NP, Hawaii (HAVO1, -6.23% yr^{-1}, $p < 0.001$), followed by Moosehorn NWR, Maine (MOOS1, -5.10% yr^{-1}, $p < 0.001$), compared to -1.4% yr^{-1} ($p = 0.002$) at Guadalupe Mountains NP, Texas (GUMO1). EC concentrations decreased at a rate greater than -2% yr^{-1} at 41 long-term sites. The weakest trends occurred at sites in the West, and sites with insignificant trends

occurred in areas influenced by biomass smoke (Bridger WA, Wyoming, BRID1; Jarbidge WA, Nevada, JARB1; and Lassen Volcanic NP, LAVO1).

Of the 136 valid short-term sites, 102 had statistically significant negative trends (Figure 6.4.1b). Sites with the strongest reductions (-5 to -6% yr^{-1}) were located in southern California, the northwestern United States, and regions of the northeastern United States. The Moosehorn NWR, Maine (MOOS1), site had the strongest reduction in EC (-7.77% yr^{-1}, $p < 0.001$) compared to -2.09% yr^{-1} ($p = 0.03$) at Big Bend NP, Texas (BIBE1). Most of the statistically insignificant trends occurred in the West at sites influenced by biomass smoke and in northern Montana and North Dakota, where oil and gas development has been demonstrated to impact EC concentrations (Gebhart et al., 2018).

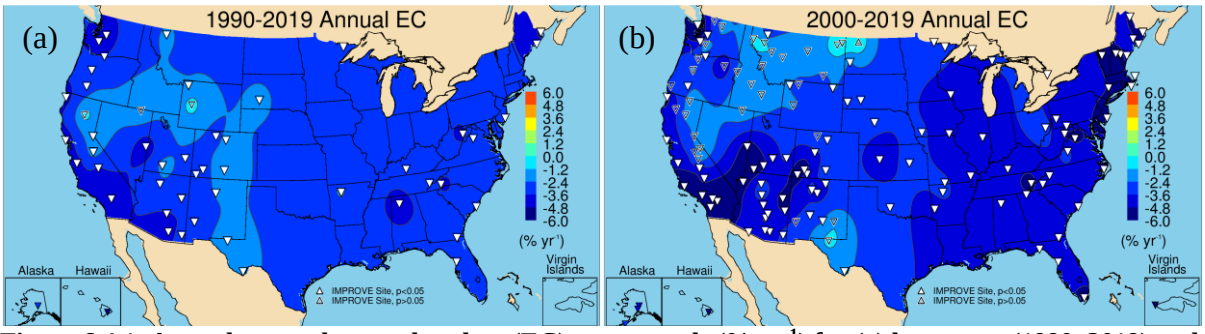

Figure 6.4.1. Annual mean elemental carbon (EC) mass trends (% yr^{-1}) for (a) long-term (1990–2019) and (b) short-term (2000–2019) periods. Filled triangles correspond to statistically significant trends ($p \leq 0.05$).

A summary of short-term regional seasonal mean trends is shown in Figure 6.4.2. Negative trends occurred for all regions and seasons. Some of the strongest reductions occurred during all seasons in the Virgin Islands region. In regions in the eastern United States, the largest negative trends occurred during summer. Trends in the Southeast region were somewhat larger than other eastern regions, especially in winter and summer. The lowest negative trends occurred in the Central region, similar to OC trends. In the West, the strongest reductions in EC occurred mainly in winter and spring (e.g., California). Negative trends in the summer were weakest, and in the Northwest region were insignificant, likely reflecting the role of biomass smoke on EC concentrations. The difference in seasonal and regional trends implies different sources influencing EC depending on region.

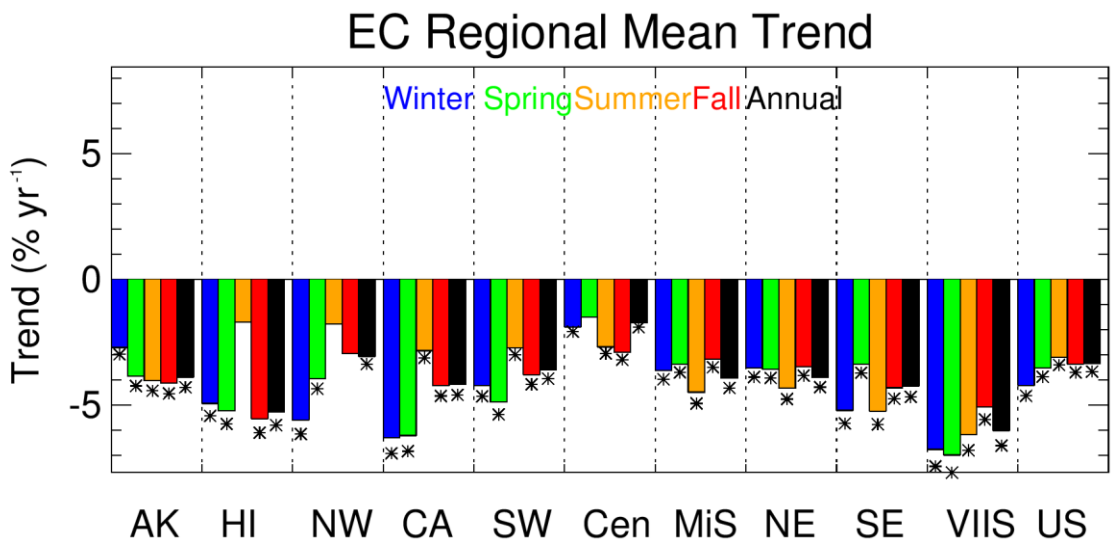

Figure 6.4.2. Short-term (2000–2019) regional seasonal mean elemental carbon (EC) trends (% yr^{-1}) for major U.S. regions for winter, spring, summer, fall, and annual means. Regions are arranged from western to eastern United States (AK = Alaska, HI = Hawaii, NW = Northwest, CA= California, SW = Southwest, Cen = Central, MiS = Midsouth, NE = Northeast, SE = Southeast, VIIS = Virgin Islands, and US = all sites). Statistically significant trends ($p \leq 0.05$) are denoted with "*".

Long-term trends in 10th and 90th percentile EC concentrations are shown in Figure 6.4.3a and 6.4.3b, respectively. The strongest reductions in the 10th percentile EC concentrations occurred at sites in the western United States. Of the 51 valid sites, 47 had statistically significant trends. Insignificant trends occurred at Bridger WA, Wyoming (BRID1); Point Reyes NP, California (PORE1); Guadalupe Mountains NP, Texas (GUMO1); and Jarbidge WA, Nevada (JARB1). The largest negative trend occurred at Hawaii Volcanoes NP, Hawaii (HAVO1, -15.46% yr^{-1}, $p = 0.006$), likely due to normalization by very low EC concentrations, followed by Three Sisters WA, Oregon (THSI1, -9.09% yr^{-1}, $p = 0.009$). The weakest negative trend occurred at Glacier NP, Montana (GLAC1, -2.16% yr^{-1}, $p = 0.003$).

The 90th percentile EC concentrations declined at all of the valid long-term sites, with 46 of the 51 sites having statistically significant trends. The strongest reductions were around -4% yr^{-1}, at sites in the northwestern United States, northeastern United States, and southern California. The strongest trend occurred at Saguaro NM, Arizona (SAGU1, -4.83% yr^{-1}, $p < 0.001$), and the weakest at Great Sand Dunes NP, Colorado (GRSA1, -0.95% yr^{-1}, $p = 0.02$). Sites in Intermountain West and parts of California corresponded to weak and insignificant trends.

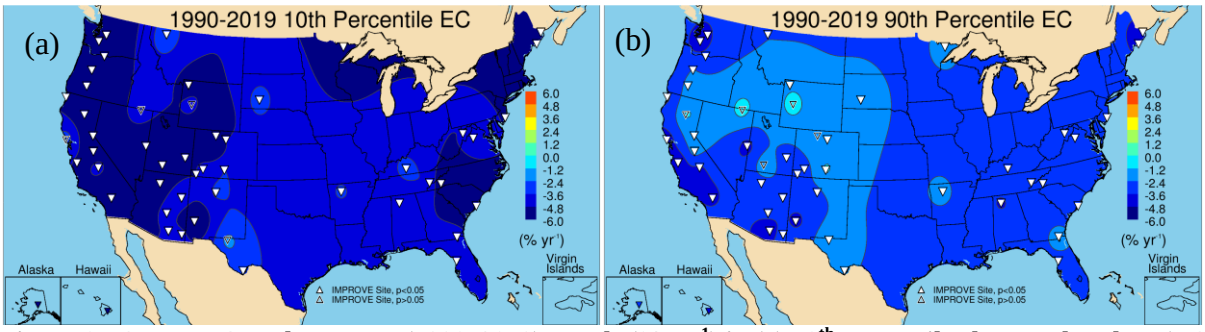

Figure 6.4.3. IMPROVE long-term (1990–2019) trends (% yr^{-1}) in (a) 10th percentile elemental carbon (EC) concentrations and (b) 90th percentile concentrations. Filled triangles correspond to statistically significant trends ($p \leq 0.05$).

Reductions in the 10th percentile EC occurred across the United States for short-term sites (Figure 6.4.4a). Recall that EC concentrations at many sites, especially in the West, may be below LQL, and therefore trends may be more uncertain. In addition, the normalized trend may be large because the normalizing concentration over the period is very low. Short-term trends in the 90th percentile EC concentrations are shown in Figure 6.4.4b. The strongest reduction occurred at San Gorgonio WA, California (SAGO1, -7.57% yr^{-1}, $p < 0.001$), compared to -1.92% yr^{-1} ($p = 0.04$) at Theodore Roosevelt NP, North Dakota (THRO1). Insignificant trends occurred at sites across the Intermountain West and northwestern United States. Some of these sites may be influenced by biomass smoke, and some, like THRO1, may be influenced by oil and gas development (Gebhart et al., 2018). Six sites in these regions had positive, although insignificant, trends. Out of the 138 valid sites, 96 had statistically significant trends. Strong reductions in 90th percentile EC occurred at sites in southern California and at sites in the northeastern and northwestern United States.

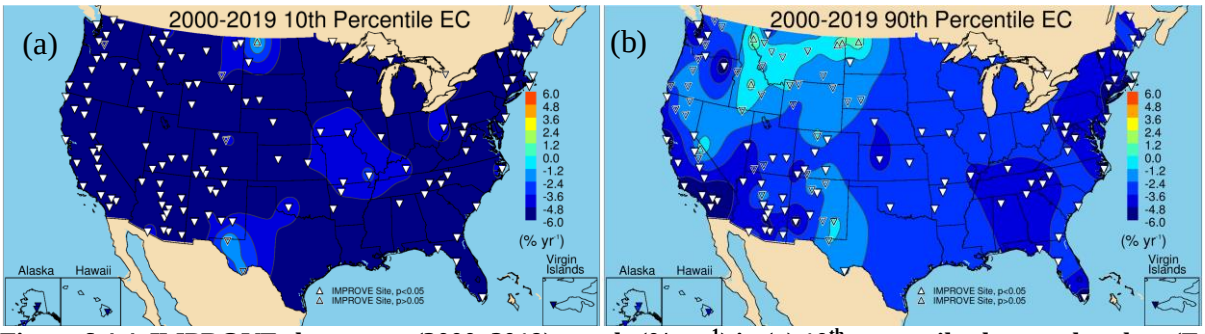

Figure 6.4.4. IMPROVE short-term (2000–2019) trends (% yr^{-1}) in (a) 10th percentile elemental carbon (EC) concentrations and (b) 90th percentile concentrations. Filled triangles correspond to statistically significant trends ($p \leq 0.05$).

Regional mean trends in percentile concentrations are shown in Figure 6.4.5. For nearly all regions, the 10th percentile trends were the greatest, although these are likely affected by low concentrations (e.g., sites in Alaska, Hawaii, and Virgin Islands). For most regions, the 90th percentile concentrations decreased at a lower rate than the median concentrations. Both the Northwest and Alaska regions had insignificant trends in 90th percentile EC concentrations, perhaps related to increased smoke impacts.

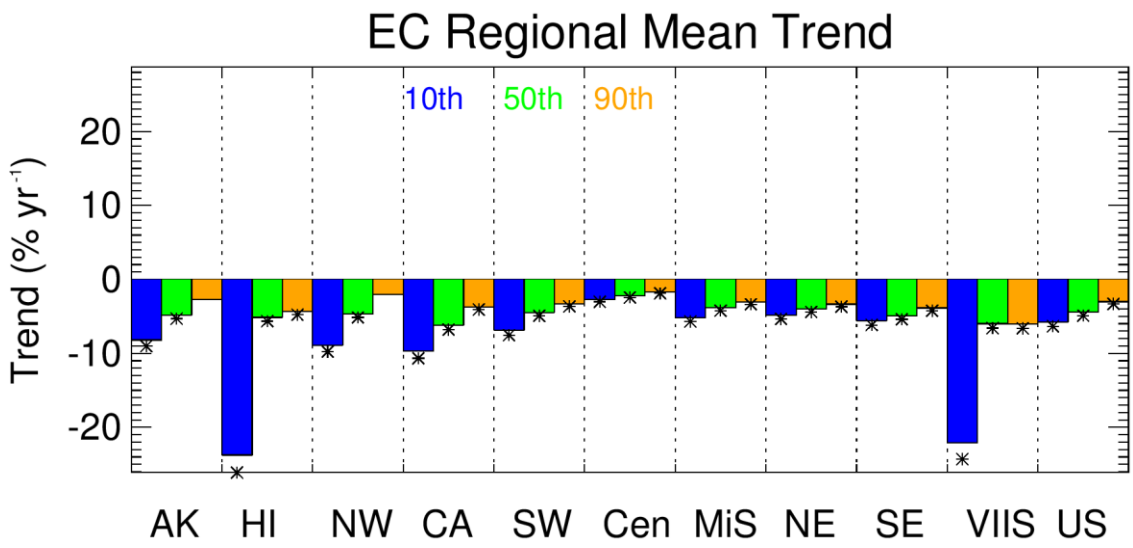

Figure 6.4.5. Short-term (2000–2019) regional mean trends (% yr^{-1}) in 10th, 50th, and 90th percentile elemental carbon (EC) percentile concentrations. Regions are arranged from western to eastern United States (AK = Alaska, HI = Hawaii, NW = Northwest, CA= California, SW = Southwest, Cen = Central, MiS = Midsouth, NE = Northeast, SE = Southeast, VIIS = Virgin Islands, and US = all sites). Statistically significant trends ($p \leq 0.05$) are denoted with "*".

6.5 FINE DUST MASS TRENDS

Recall from Chapter 2.1 that FD concentrations were determined by combining the oxides of elemental mass concentrations of Al, Si, Ca, Fe, and Ti (see Table 2.1). The analytical methods used to determine these species have evolved over time and included PIXE (proton induced X-ray emission) and XRF (X-ray fluorescence) techniques. The transitions from PIXE to XFR methods, the change in XRF anodes from Mo to Cu, as well as different calibration procedures affect the data by changing MDLs (Hyslop et al., 2015). In 2011, the analysis method switched to the PANalytical XRF system that resolved issues related to undetected Al with concentrations above the MDL (White, 2006). Before 2011, XRF data below the MDL were replaced by 0.5×MDL. Changes in analytical methods may not equally affect data for each FD species; therefore, the integrated dust concentration may be less susceptible to possible variability introduced by the analytical methods, although this has not been specifically demonstrated.

Long-term and short-term annual mean FD trends are shown in Figures 6.5.1a and 6.5.1b, respectively. Roughly 40% of long-term trends were insignificant (23 out of 56 valid sites); nearly all of these were located at sites in the western United States, and many (12) of them were positive. In the West, statistically significant reductions in FD occurred in California, Oregon, Washington State, Wyoming, and Colorado. Across the eastern United States, FD decreased at all sites. The strongest reductions occurred at Yellowstone NP, Wyoming (YELL1, -3.94% yr^{-1}, $p < 0.001$), compared to an increase in FD at Guadalupe Mountains NP, Texas (GUMO1, 1.22% yr^{-1}, $p = 0.05$).

Annual mean trends in FD for 2000–2019 were significantly negative at sites across the eastern United States, especially at sites in the northeastern United States, and across the Intermountain West and northwestern United States. Out of 134 sites, 68 had statistically significant trends. These ranged from -6.04% yr^{-1} ($p < 0.001$) in Great Gulf WA, New Hampshire (GRGU1), to -1.57% yr^{-1} ($p = 0.03$) at Northern Cheyenne, Montana (NOCH1). Many of the insignificant trends were positive (11) at sites near the Central Valley of California, Oklahoma, Texas, Oregon, and North Dakota. Many of the sites in the southwestern United States had statistically insignificant trends.

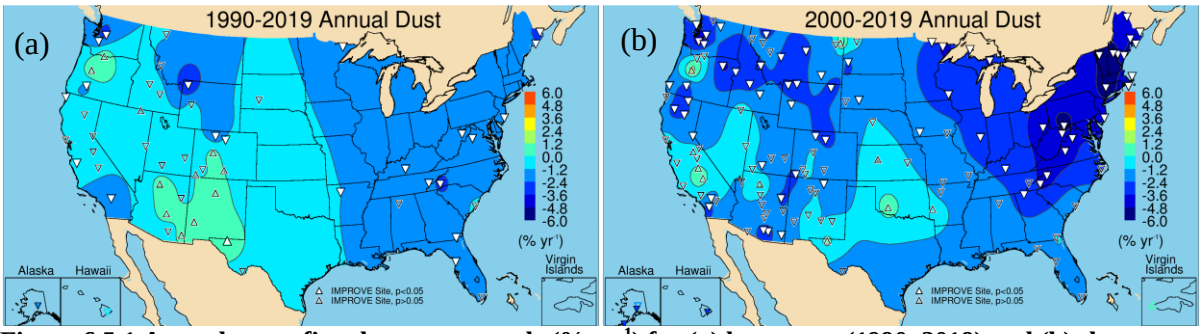

Figure 6.5.1 Annual mean fine dust mass trends (% yr^{-1}) for (a) long-term (1990–2019) and (b) short-term (2000–2019) periods. Filled triangles correspond to statistically significant trends ($p \leq 0.05$).

Compared to other species, trends in FD showed greater seasonal and spatial variability. Trends were mostly insignificant and generally not strongly negative as is the case for other species. The Northeast region was the only region with statistically significant trends during all seasons. The Southeast region had statistically significant reductions in FD during all seasons except summer. Similarly, the Midsouth region had insignificant but positive trends during summer; this is the season with impacts from North African dust transport. In the Central region, only winter and spring corresponded to statistically significant negative trends. Across the West, regions were associated with insignificant though negative trends. The California region had insignificant but positive trends during summer, and the summer trends in the Northwest region were flat. FD has not experienced the levels of reduction that have occurred for other species.

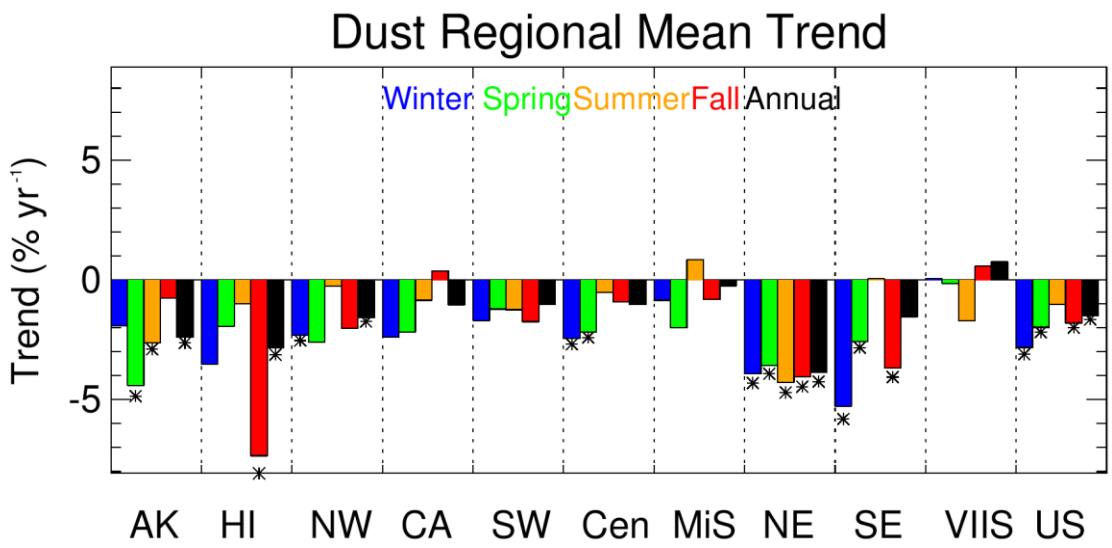

Figure 6.5.2. Short-term (2000–2019) regional seasonal mean fine dust mass trends (% yr^{-1}) for major U.S. regions for winter, spring, summer, fall, and annual means. Regions are arranged from western to eastern United States (AK = Alaska, HI = Hawaii, NW = Northwest, CA= California, SW = Southwest, Cen = Central, MiS = Midsouth, NE = Northeast, SE = Southeast, VIIS = Virgin Islands, and US = all sites). Statistically significant trends ($p \leq 0.05$) are denoted with "*".

Long-term trends in the 10th percentile FD concentrations are shown in Figure 6.5.3a. For most of the United States, sites experienced reductions in the lowest FD concentrations. Of the 59 valid sites, 46 had statistically significant trends, ranging from -6.25% yr^{-1} ($p < 0.001$) in Three Sisters WA, Oregon (THSI1), to 1.80% yr^{-1} ($p = 0.010$) in Guadalupe Mountains NP, Texas (GUMO1). All of the insignificant trends occurred at sites in the southwestern United States. In contrast, for the 90th percentile, of the 59 valid sites only 17 had statistically significant trends, and many of these sites were in the eastern United States (Figure 6.5.3b). Sites across the southwestern United States were associated with positive although insignificant trends. Trends in the 90th percentile FD ranged from -3.78% yr^{-1} ($p < 0.001$) at Yellowstone NP, Wyoming (YELL1), to 2.38% yr^{-1} ($p = 0.011$) at Columbia River Gorge, Washington (CORI1).

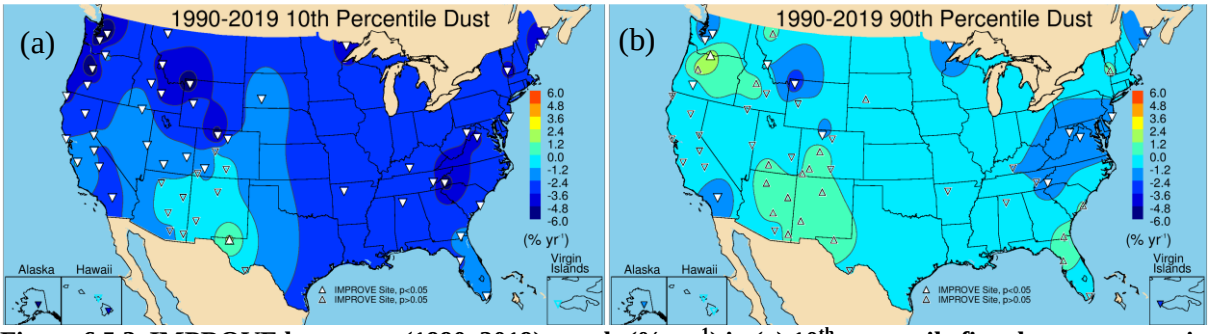

Figure 6.5.3. IMPROVE long-term (1990–2019) trends (% yr^{-1}) in (a) 10th percentile fine dust concentrations and (b) 90th percentile concentrations. Filled triangles correspond to statistically significant trends ($p \leq 0.05$).

Short-term trends in 10th percentile FD concentrations were negative at sites across the United States, with stronger reductions across the eastern and Intermountain West and

northwestern United States (Figure 6.5.4a). Insignificant trends occurred at 34 sites out of 137 valid sites, and most of these were in the southwestern United States. Trends ranged from -9.34% yr^{-1} ($p = 0.006$) at White Pass, Washington (WHPA1), to -1.72% yr^{-1} ($p = 0.019$) at Pinnacles NM, California (PINN1).

Most of the short-term 90th percentile trends in FD at sites in the West were insignificant (Figure 6.5.4b), with 84 insignificant trends out of 137 valid sites. Positive though insignificant trends occurred at sites in the central United States, the Central Valley of California, Oregon, the northern Great Plains, and Florida. The 90th percentile trends ranged from -6.67% yr^{-1} ($p < 0.001$) at Great Gulf WA, New Hampshire (GRGU1), to -1.18% yr^{-1} ($p = 0.013$) at Viking Lake, Iowa (VILA1). Comparisons of trends from these two maps suggests that the influences that govern the FD trend 10th and 90th percentiles are different, although low 10th percentile concentrations could also play a role.

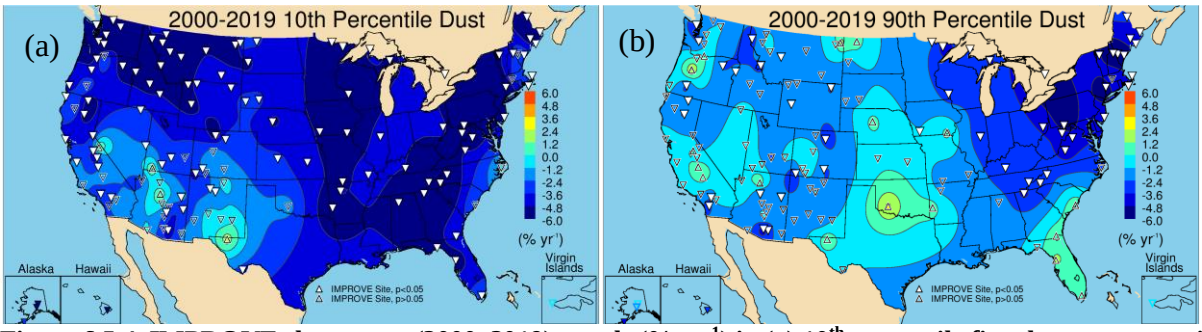

Figure 6.5.4. IMPROVE short-term (2000–2019) trends (% yr^{-1}) in (a) 10th percentile fine dust concentrations and (b) 90th percentile concentrations. Filled triangles correspond to statistically significant trends ($p \leq 0.05$).

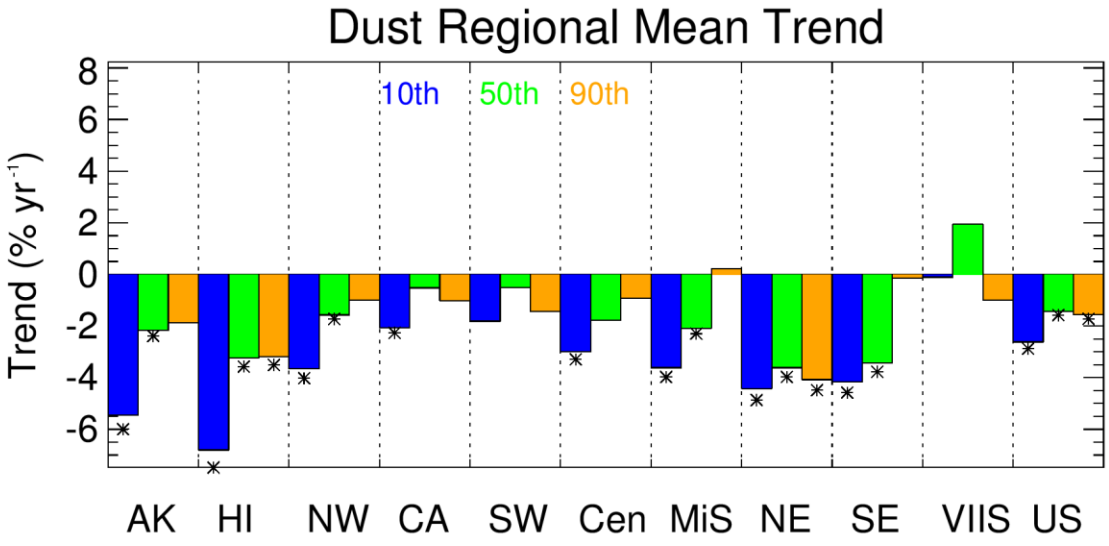

Figure 6.5.5. Short-term (2000–2019) regional mean trends (% yr^{-1}) trends in 10th, 50th, and 90th percentile fine dust concentrations. Regions are arranged from western to eastern United States (AK = Alaska, HI = Hawaii, NW = Northwest, CA= California, SW = Southwest, Cen = Central, MiS = Midsouth, NE = Northeast, SE = Southeast, VIIS = Virgin Islands, and US = all sites). Statistically significant trends ($p \leq 0.05$) are denoted with "*".

For most regions, the 10th percentile FD trends were strongest, which may be in part due to low 10th percentile FD concentrations (Figure 6.5.5). For nearly all regions, the 90th percentile trends were insignificant (except the Northeast and Hawaii regions). These insignificant trends may imply that the influences on the highest FD concentrations have not decreased steadily to result in statistically significant negative trends. For other regions in the West, such as the California, Southwest, and Central regions, the median trends were also insignificant.

6.6 GRAVIMETRIC $PM_{2.5}$ FINE MASS TRENDS

Trends in $PM_{2.5}$ fine mass (FM) may be driven by trends in a particular species, depending on the degree of its contribution; however, inferring FM trends based on the trends of other species is complicated because of the spatial and seasonal variability of a specific species relative to another. The statistical significance level of trends at a given site differs for each species and for FM trends, complicating comparisons of trends from different species at a specific location. In addition, sampling or analytical artifacts, such as particle bound water, may influence FM trends (see Chapter 1, Section 1.3.1.2). For example, beginning in 2011, higher laboratory relative humidity during weighing resulted in an increase in particle bound water associated with FM data (White, 2016). This issue was resolved in 2019, but it may influence trends in FM (Hand et al., 2019).

Long-term trends in annual mean FM are shown in Figure 6.6.1a. Of the 56 valid sites, 44 had statistically significant trends, ranging from -4.39% yr^{-1} ($p < 0.001$) at Shining Rock WA, North Carolina (SHRO1), to -0.85% yr^{-1} ($p < 0.001$) at Tonto NM, Arizona (TONT1). The strongest trends occurred at sites in the eastern United States, likely associated with reductions in sulfate concentrations (see Figure 6.1.1a). Most of the insignificant trends occurred in the western United States, similar to trends in OC (Figure 6.3.1a).

Short-term trends in annual mean FM are shown in Figure 6.6.1b. The spatial pattern in short-term trends follows that of long-term trends, with the strongest reduction in FM at sites in the eastern United States, again, likely associated with sulfate reductions. Of the 134 valid short-term sites, only 78 were associated with statistically significant trends, and nearly all of the insignificant trends occurred at sites in the western United States, especially at sites in the Intermountain West, northwestern United States, and northern California, where OC trends were also insignificant. Sites in southern California had strong negative trends, likely associated with nitrate ion reductions. The short-term trends ranged from -5.79% yr^{-1} ($p < 0.001$) at Frostburg Reservoir, Maryland (FRRE1), to -1.02 % yr^{-1} ($p = 0.016$) at Theodore Roosevelt NP, North Dakota (THRO1).

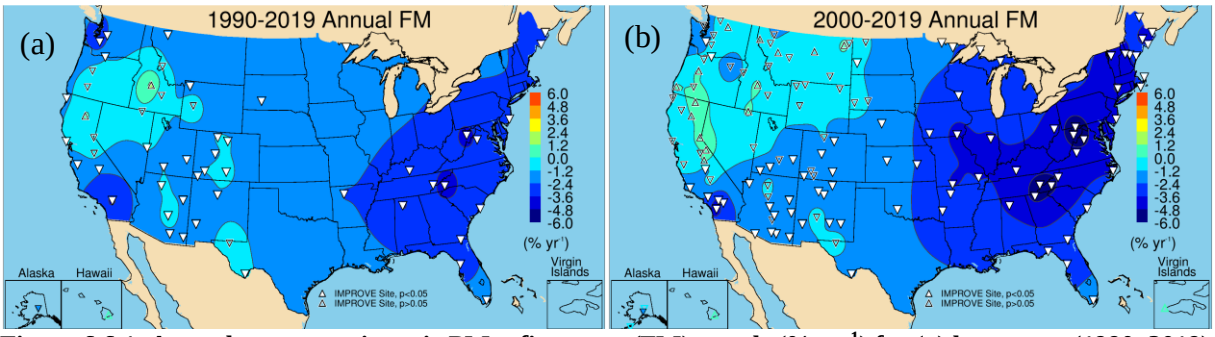

Figure 6.6.1. Annual mean gravimetric $PM_{2.5}$ fine mass (FM) trends (% yr^{-1}) for (a) long-term (1990–2019) and (b) short-term (2000–2019) periods. Filled triangles correspond to statistically significant trends ($p \leq 0.05$).

The short-term regional seasonal mean trends in the eastern United States were similar to regional seasonal mean sulfate trends (compare Figure 6.6.2 to Figure 6.1.2). The strongest reductions in FM occurred in the Northeast and Southeast regions (-4% yr^{-1} to -5% yr^{-1}). Trends were weaker moving west, and in regions such as the Northwest and California, FM trends were similar to OC trends. Summer and fall trends in these regions were insignificant and positive, indicating the role of biomass smoke in FM trends. In the Southwest region, all of the seasons except summer had statistically significant reductions in FM. Only summer had an insignificant (negative) trend, similar to both OC and FD trends.

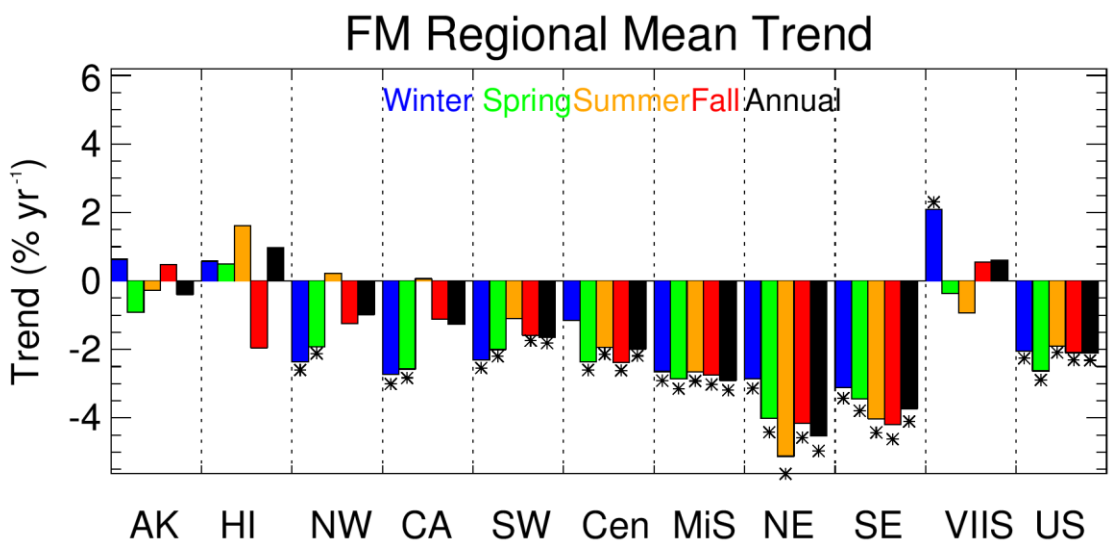

Figure 6.6.2. Short-term (2000–2019) regional seasonal mean gravimetric $PM_{2.5}$ fine mass (FM) trends (% yr^{-1}) for major U.S. regions for winter, spring, summer, fall, and annual means. Regions are arranged from western to eastern United States (AK = Alaska, HI = Hawaii, NW = Northwest, CA= California, SW = Southwest, Cen = Central, MiS = Midsouth, NE = Northeast, SE = Southeast, VIIS = Virgin Islands, and US = all sites). Statistically significant trends ($p \leq 0.05$) are denoted with "*".

Long-term trends in 10th percentile FM concentrations are shown in Figure 6.6.3a. All but four of the 58 valid sites had statistically significant trends. The lowest reductions occurred at sites in California and in the southwestern United States. The strongest reductions occurred at

Snoqualmie Pass, Washington (SNPA1, -5.93% yr^{-1}, $p < 0.001$), and the weakest reductions occurred at Guadalupe Mountains NP, Texas (GUMO1, -0.75% yr^{-1}, $p = 0.05$).

The long-term 90th percentile trends are shown in Figure 6.6.3b. More sites had insignificant trends (19 sites) and most of them were in the western United States, especially in the northwestern United States, likely influenced by OC trends given similarities in their spatial patterns. Strong reductions at sites in the eastern United States were likely influenced by sulfate reductions. The trends in 90th percentile FM ranged from -4.83% yr^{-1} ($p < 0.001$) at Shining Rock WA, North Carolina (SHRO1), to -0.71% yr^{-1} ($p = 0.02$) at Tonto NM, Arizona (TONT1); these maximum and minimum trends occurred at the same sites as for annual mean trends.

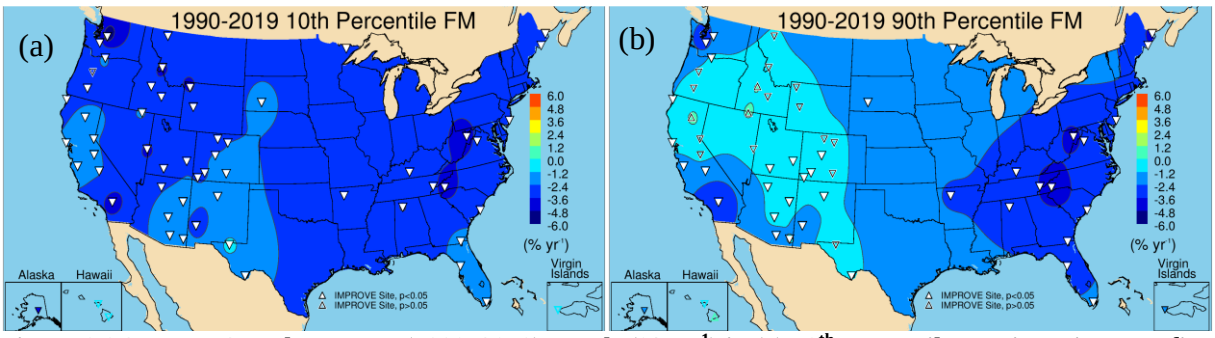

Figure 6.6.3. IMPROVE long-term (1990–2019) trends (% yr^{-1}) in (a) 10th percentile gravimetric $PM_{2.5}$ fine mass (FM) concentrations and (b) 90th percentile concentrations. Filled triangles correspond to statistically significant trends ($p \leq 0.05$).

Of the 137 valid short-term sites for the 10th percentile trends in FM, 101 were statistically significant (Figure 6.6.4a). All of the trends for sites in the eastern United States were negative and statistically significant, with the strongest reductions at sites along the Ohio River valley and Appalachia areas. Reductions also occurred at sites in the northwestern United States. Insignificant trends occurred at sites in California and Oregon. Trends in the 10th percentile FM ranged from -5.31% yr^{-1} ($p < 0.001$) at Dolly Sods WA, West Virginia (DOSO1), to -1.14% yr^{-1} ($p = 0.03$) at Organ Pipe, Arizona (ORPI1).

Spatial patterns in the short-term 90th percentile FM trends were similar to those for OC trends in the western United States and sulfate trends in the eastern United States (Figure 6.6.4b). The strongest reductions occurred at sites in the East (-8.36% yr^{-1}, $p < 0.001$ at Frostburg Reservoir, Maryland, FRRE1). Of the 137 valid sites, 67 had trends that were statistically insignificant, and nearly all of these occurred in the western United States, especially in the northwestern United States, California, and Oregon, where biomass smoke has influenced OC as well as FM trends. The weakest reduction occurred at Voyageurs NP, Minnesota, (VOYA2, -0.78% yr^{-1}, $p = 0.04$).

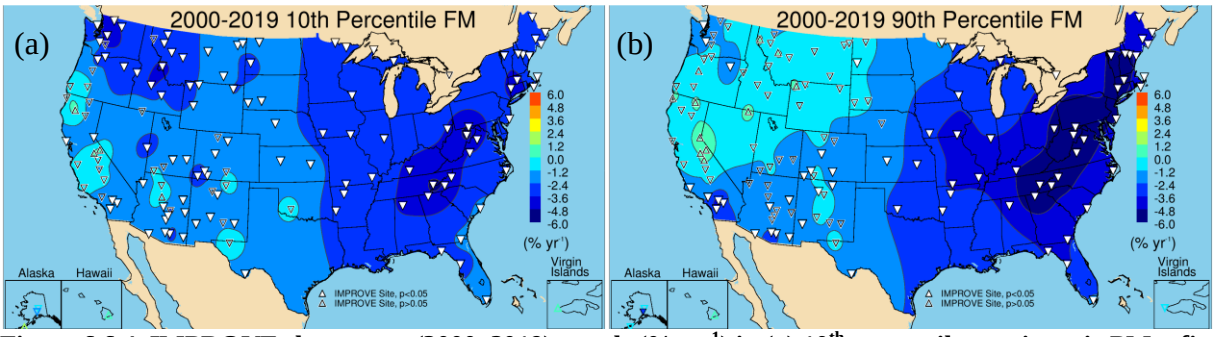

Figure 6.6.4. IMPROVE short-term (2000–2019) trends (% yr^{-1}) in (a) 10th percentile gravimetric $PM_{2.5}$ fine mass (FM) concentrations and (b) 90th percentile concentrations. Filled triangles correspond to statistically significant trends ($p \leq 0.05$).

The strongest short-term regional FM percentile trends occurred in the Northeast and Southeast regions (Figure 6.6.5). In both regions, the 90th percentile FM concentrations decreased most strongly (-4% yr^{-1} to -5% yr^{-1}), especially in the Northeast region, likely related to sulfate reductions. Recall that the summer seasonal mean trends were also greatest in the Northeast region (Figure 6.6.2). In the western United States, 90th percentile reductions were either insignificant and/or the lowest of the 10th and 50th percentiles, due to the impacts of OC trends from biomass smoke influence. In both the Northwest and Southwest regions, the lowest FM concentrations decreased at a faster rate. Trends at OCONUS regions (outside CONUS) were insignificant.

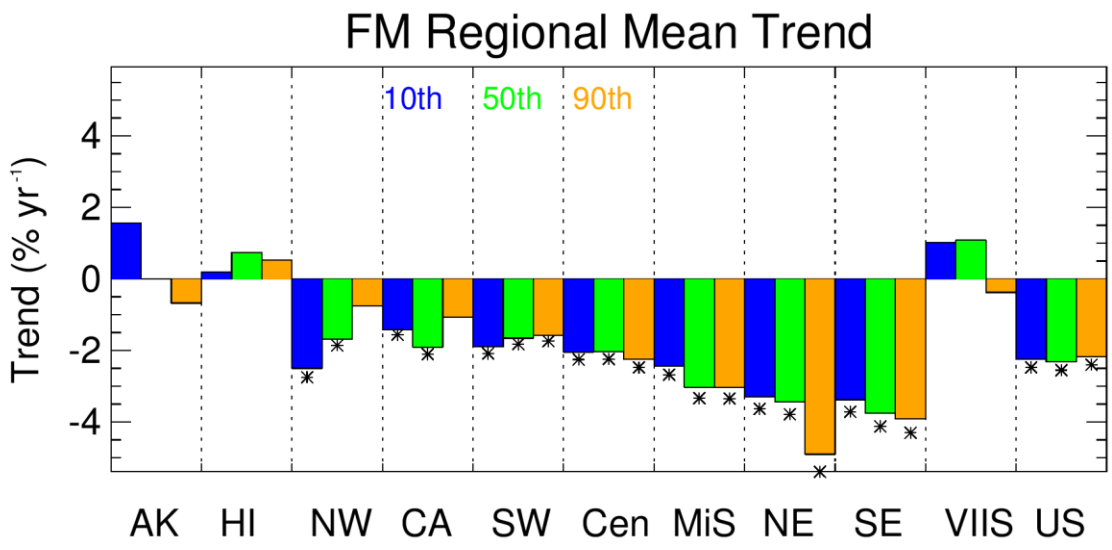

Figure 6.6.5. Short-term (2000–2019) regional mean trends (% yr^{-1}) in 10th, 50th, and 90th percentile gravimetric $PM_{2.5}$ fine mass (FM) concentrations. Regions are arranged from western to eastern United States (AK = Alaska, HI = Hawaii, NW = Northwest, CA= California, SW = Southwest, Cen = Central, MiS = Midsouth, NE = Northeast, SE = Southeast, VIIS = Virgin Islands, and US = all sites). Statistically significant trends ($p \leq 0.05$) are denoted with "*".

6.7 PM_{10} TRENDS

PM_{10} concentrations are determined gravimetrically and correspond to particles with an aerodynamic diameter less than 10 µm. PM_{10} mass concentrations include all the species presented in the previous sections, in addition to coarse mass, and are similar to $PM_{2.5}$ trends except for when contributions from CM are significant.

The spatial pattern in long-term annual mean PM_{10} trends was similar to the annual mean FM trends pattern (Figure 6.7.1a). The strongest reductions occurred at sites in the eastern United States and in southern California. Of the 49 valid sites, 37 had statistically significant trends. Sites with lower and insignificant trends occurred in California, Oregon, and Nevada, similar to FM trends. However, unlike for FM trends, sites in the southwestern United States also had insignificant trends, likely associated with CM. Trends in PM_{10} ranged from -3.70% yr^{-1} ($p < 0.001$) at Dolly Sods WA, West Virginia (DOSO1), to -0.93% yr^{-1} ($p = 0.02$) at Big Bend NP, Texas (BIBE1).

The differences in trends between the eastern and western United States also existed for short-term trends in annual mean PM_{10}, with the strongest trends at sites in the eastern United States, due to sulfate reductions (Figure 6.7.1b). Positive but insignificant trends occurred at sites in California, Oregon, Washington, northern Montana, and North Dakota. This spatial pattern was similar to FM trends, except for the addition of insignificant PM_{10} trends at sites in the southwestern and central United States, likely associated with CM. The strongest reduction occurred at Frostburg Reservoir, Maryland (FRRE1, -4.02% yr^{-1}, $p < 0.001$), and annual mean PM_{10} increased at Three Sisters WA, Oregon (1.73% yr^{-1}, $p = 0.03$).

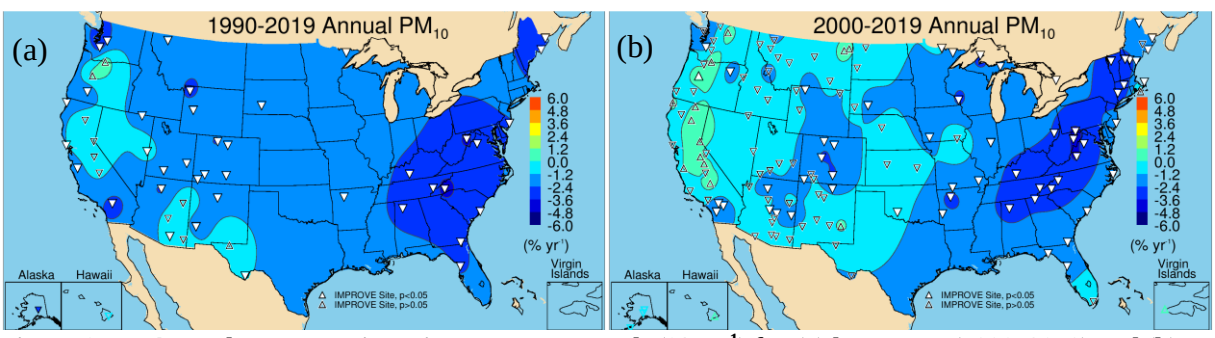

Figure 6.7.1. Annual mean gravimetric PM_{10} mass trends (% yr^{-1}) for (a) long-term (1990–2019) and (b) short-term (2000–2019) periods. Filled triangles correspond to statistically significant trends ($p \leq 0.05$).

Comparisons of short-term regional and seasonal mean trends in PM_{10} are shown in Figure 6.7.2. The strong reductions in PM_{10} in eastern regions (-2% yr^{-1} to -3% yr^{-1}) were similar to those for FM, suggesting that in the Northeast and Southeast regions, PM_{10} trends were largely driven by FM species. None of the seasonal mean trends in the Central region was statistically significant, unlike for FM trends, suggesting the additional role of CM in that region. This was also apparent for the Southwest region. In the California region, both winter and spring PM_{10} and FM trends were similar, suggesting trends in those seasons were driven by FM trends. However, summer and fall PM_{10} trends in the California region were flat and insignificant, while FM trends were either flat or negative but insignificant. All of the seasonal mean trends in the Southwest region were insignificant, unlike FM trends.

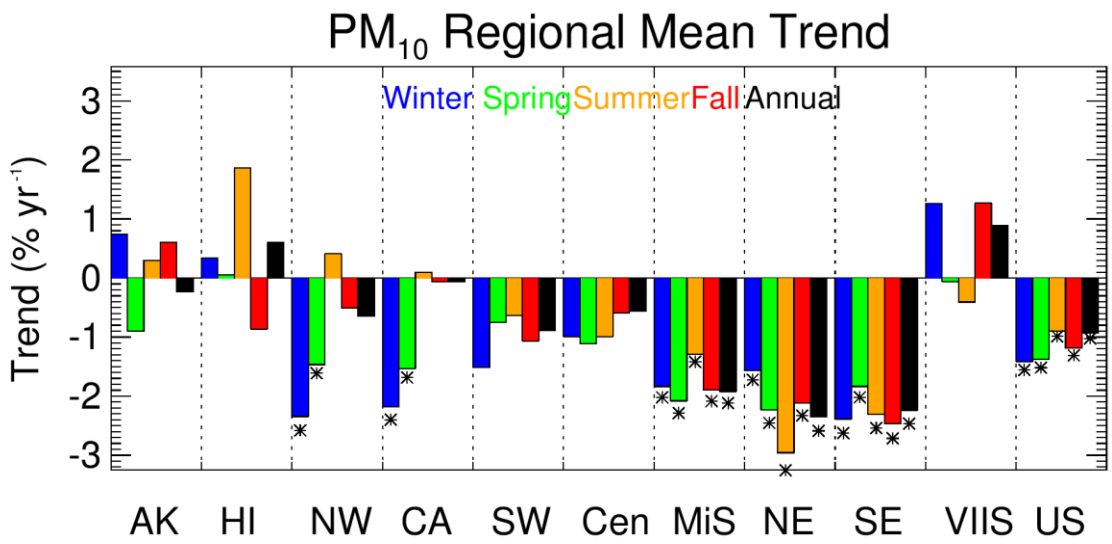

Figure 6.7.2. Short-term (2000–2019) regional seasonal mean gravimetric PM_{10} mass trends (% yr^{-1}) for major U.S. regions for winter, spring, summer, fall, and annual means. Regions are arranged from western to eastern United States (AK = Alaska, HI = Hawaii, NW = Northwest, CA= California, SW = Southwest, Cen = Central, MiS = Midsouth, NE = Northeast, SE = Southeast, VIIS = Virgin Islands, and US = all sites). Statistically significant trends ($p \leq 0.05$) are denoted with "*".

The long-term 10th percentile trends in PM_{10} are shown in Figure 6.7.3a. Nearly all of the trends at 50 valid sites were statistically significant, with the only insignificant trend at Guadalupe Mountains NP, Texas (GUMO1). The strongest reductions occurred at sites in the Intermountain West and Northwest, and trends ranged from -7.40% yr^{-1} ($p < 0.001$) at Mount Zirkel WA, Colorado (MOZI1), to -1.52% yr^{-1} ($p < 0.001$) at Saguaro NM, Arizona (SAGU1).

The long-term 90th percentile trends in PM_{10} (Figure 6.7.3b) were similar to the 90th percentile FM trends, with the strong reductions at sites in the eastern United States, and were likely driven by reductions in FM and specifically sulfate. Most of the sites in the West had insignificant trends (32 out of 50 valid sites had statistically significant trends). Most of these trends occurred at sites in California, Oregon, and the southwestern United States. Trends ranged from -4.03% yr^{-1} ($p < 0.001$) at Shining Rock WA, North Carolina (SHRO1), to 1.70% yr^{-1} ($p = 0.014$) at Columbia River Gorge, Washington (CORI1). This site had the only statistically significant positive trend and was negative for FM, suggesting that CM played an important role.

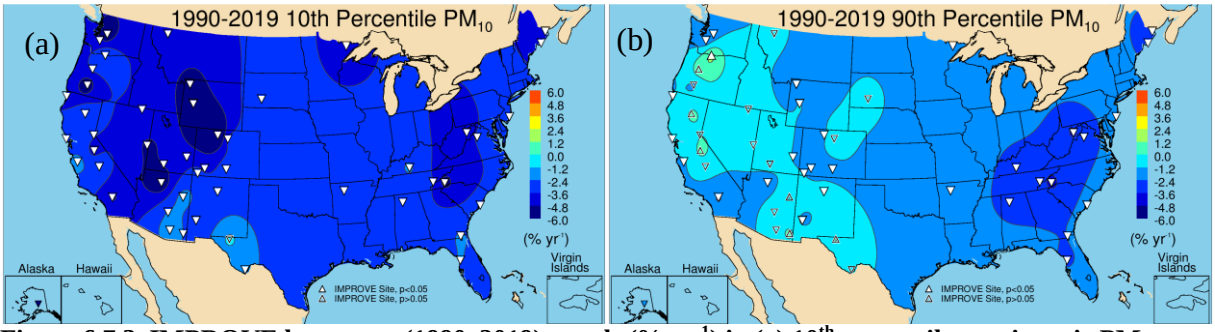

Figure 6.7.3. IMPROVE long-term (1990–2019) trends (% yr^{-1}) in (a) 10th percentile gravimetric PM_{10} mass concentrations and (b) 90th percentile concentrations. Filled triangles correspond to statistically significant trends ($p \leq 0.05$).

The short-term 10th percentile PM_{10} concentrations declined significantly at most valid sites (Figure 6.7.4a), especially at sites in the eastern United States. However, unlike FM trends, many sites in the southwestern United States had insignificant trends in PM_{10}. Out of 137 valid sites, 78 were statistically significant, but many insignificant trends occurred at sites in California or the southwestern United States. Trends ranged from -4.35% yr^{-1} ($p = 0.002$) at Olympic, Washington (OLYM1), to -0.77% yr^{-1} ($p = 0.046$) at San Pedro Parks, New Mexico (SAPE1).

The spatial pattern in the short-term 90th percentile PM_{10} trends was similar to the FM trends (Figure 6.7.4b), with the exception of sites in the southwestern and central United States. At sites in these areas, trends were flat and insignificant. Three sites had statistically significant positive trends, including Lassen Volcanic NP, California (LAVO1, 1.64% yr^{-1}, $p = 0.03$), Three Sisters WA, Oregon (THSI1, 2.26% yr^{-1}, $p = 0.004$), and Columbia River Gorge, Washington (CORI1, 2.42% yr^{-1}, $p = 0.03$). The largest negative trend occurred at Frostburg Reservoir, Maryland (FRRE1, -4.76% yr^{-1}, $p < 0.001$), similar to FM trends.

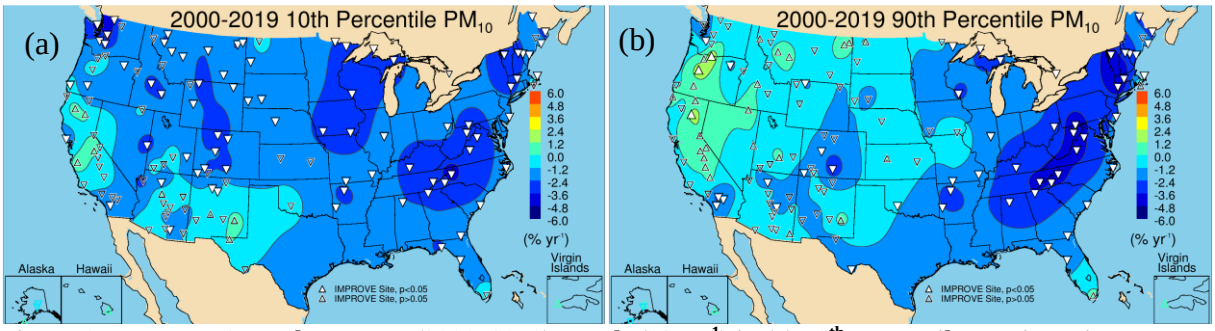

Figure 6.7.4. IMPROVE short-term (2000–2019) trends (% yr^{-1}) in (a) 10th percentile gravimetric PM_{10} mass concentrations and (b) 90th percentile concentrations. Filled triangles correspond to statistically significant trends ($p \leq 0.05$).

Both of the PM_{10} regional mean trends in the Northeast and Southeast regions were similar to FM trends, with the 90th percentile PM_{10} concentration trends being the largest, which were likely driven by reductions in FM, specifically sulfate (Figure 6.7.5). In the Central region, only the 10th percentile trends were significant, unlike for FM when all percentile trends were significant, suggesting additional influence on the 50th and 90th percentile trends. Similar results occurred in the Southwest and California regions, where none of the PM_{10} trends was significant

but nearly all of the FM trends were. Trends in the Northwest region were similar for PM_{10} and FM, suggesting that PM_{10} trends were driven by FM trends.

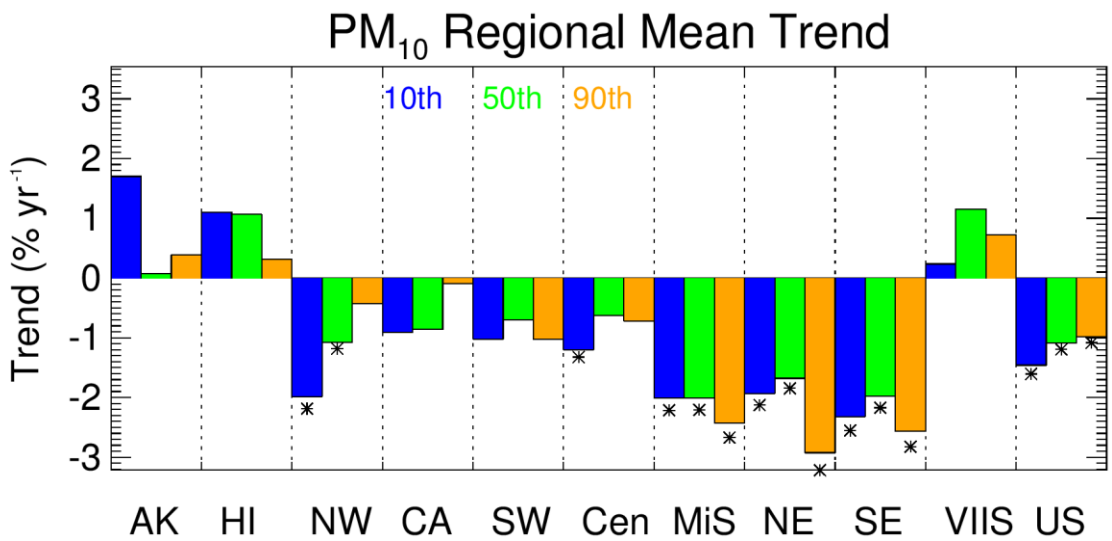

Figure 6.7.5. Short-term (2000–2019) regional mean trends (% yr^{-1}) in 10th, 50th, and 90th percentile gravimetric PM_{10} mass concentrations. Regions are arranged from western to eastern United States (AK = Alaska, HI = Hawaii, NW = Northwest, CA= California, SW = Southwest, Cen = Central, MiS = Midsouth, NE = Northeast, SE = Southeast, VIIS = Virgin Islands, and US = all sites). Statistically significant trends ($p \leq 0.05$) are denoted with "*".

6.8 COARSE MASS TRENDS

CM is calculated as the difference between PM_{10} and $PM_{2.5}$ (FM) gravimetric mass. CM is often associated with mechanically generated sources and assumed to be composed of mineral dust, but as discussed in Section 2.2.12, it can also include carbonaceous and inorganic ion material. Spatial patterns in CM trends may be similar to FD trends, assuming FD is the tail of the coarse dust mode, but could vary if CM is composed of material other than mineral dust, or if the coarse mode size distribution is shifted to a larger size.

Annual mean long-term trends in CM are shown in Figure 6.8.1a. The strongest reductions in CM occurred at sites in Wyoming and Colorado. Of the 49 valid sites, 30 of them had statistically significant trends. Insignificant trends mostly occurred at sites in the western United States, in California, Arizona, and Texas. One positive trend occurred at Columbia River Gorge, Washington (CORI1, 1.83% yr^{-1}, $p = 0.04$). The strongest reduction in CM occurred at Crater Lake NP, Oregon (CRLA1, -5.39% yr^{-1}, $p < 0.001$).

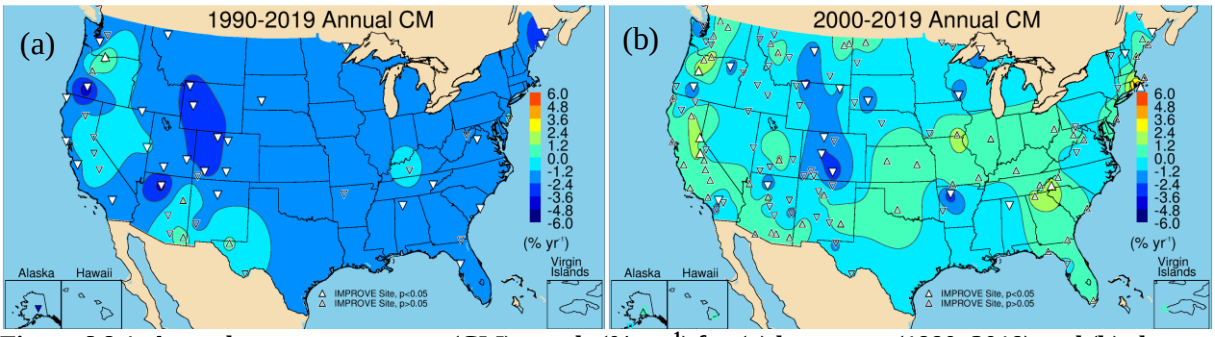

Figure 6.8.1. Annual mean coarse mass (CM) trends (% yr^{-1}) for (a) long-term (1990–2019) and (b) short-term (2000–2019) periods. Filled triangles correspond to statistically significant trends ($p \leq 0.05$).

Short-term annual mean CM trends are shown in Figure 6.8.1b. Only 23 of 131 valid sites had statistically significant trends, suggesting that at most sites, trends were variable. CM declined significantly at some sites, for example, in Colorado, Wyoming, and Montana, and in Arkansas, where the strongest reductions occurred at Upper Buffalo WA, Arkansas (UPBU1 -3.85% yr^{-1}, $p = 0.045$). Positive trends (mostly insignificant) occurred at 61 sites, with six being statistically significant (Martha's Vineyard, Massachusetts, MAVI1; Shining Rock WA, North Carolina, SHRO1; Three Sisters WA, Oregon, THSI1; Yosemite NP, California, YOSE1; Bliss SP, California, BLIS1; and Trapper Creek, Alaska, TRCR1). The spatial pattern in short-term CM trends was different from FD trends (Figure 6.5.1b), suggesting that different composition or size distribution of coarse-mode aerosols influenced CM trends.

Regional seasonal mean trends are shown in Figure 6.8.2. As suggested in Figure 6.8.1b, nearly all of the regions were associated with insignificant and weak trends, especially relative to other species already discussed. The Northeast region had significant positive trends in summer, as did the Alaska and Hawaii regions. All of the seasonal mean trends in the Central region were positive but insignificant. The Midsouth and Southwest regions had weak but negative insignificant trends, while the California region had weak, positive insignificant trends in summer and fall but negative, insignificant trends in winter and spring, The Northwest region had statistically significant trends in winter but weak and insignificant trends during other seasons.

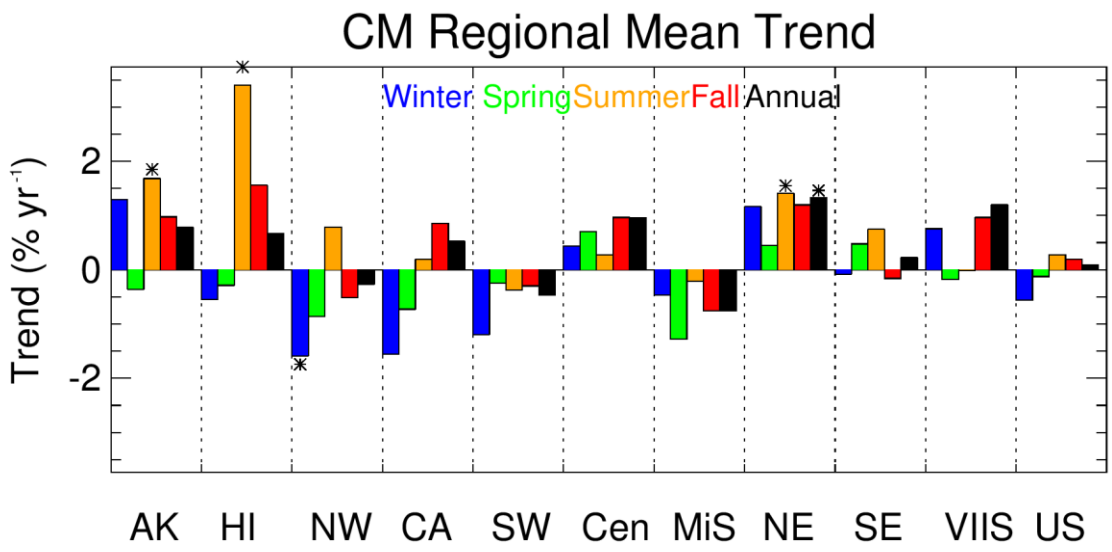

Figure 6.8.2. Short-term (2000–2019) regional seasonal mean coarse mass (CM) trends (% yr^{-1}) for major U.S. regions for winter, spring, summer, fall, and annual means. Regions are arranged from western to eastern United States (AK = Alaska, HI = Hawaii, NW = Northwest, CA= California, SW = Southwest, Cen = Central, MiS = Midsouth, NE = Northeast, SE = Southeast, VIIS = Virgin Islands, and US = all sites). Statistically significant trends ($p \leq 0.05$) are denoted with "*".

The 10th percentile long-term trends were negative at most sites (44 out of 50 valid sites), with the strongest reductions at sites in the Intermountain West and southwestern United States (Figure 6.8.3a). Of the 50 valid sites, 31 had statistically significant trends, ranging from -8.94% yr^{-1} ($p < 0.001$) at Mount Zirkel WA, Colorado (MOZI1), to -1.64% yr^{-1} ($p = 0.016$) at Tonto NM, Arizona (TONT1). The trends in 90th percentile CM did not decrease to the same degree as the 10th percentile trends (Figure 6.8.3b). Of the 50 valid sites, 30 had statistically significant trends, ranging from -5.32% yr^{-1} ($p < 0.001$) at Crater Lake NP, Oregon (CRLA1), to 2.82% yr^{-1} ($p = 0.002$) at Columbia River Gorge, Washington (CORI1). Recall that the 90th percentile trend in FD at CRLA1 was also positive, suggesting CM is likely associated with mineral dust at this site. The 90th percentile CM trends decreased at a higher rate than the 90th percentile FD trends, especially for sites in the southwestern United States. Similarities in FD and CM trends occurred for sites in Arizona and Texas. Insignificant positive 90th percentile CM trends at sites in California were insignificant but negative for the 90th percentile FD trends.

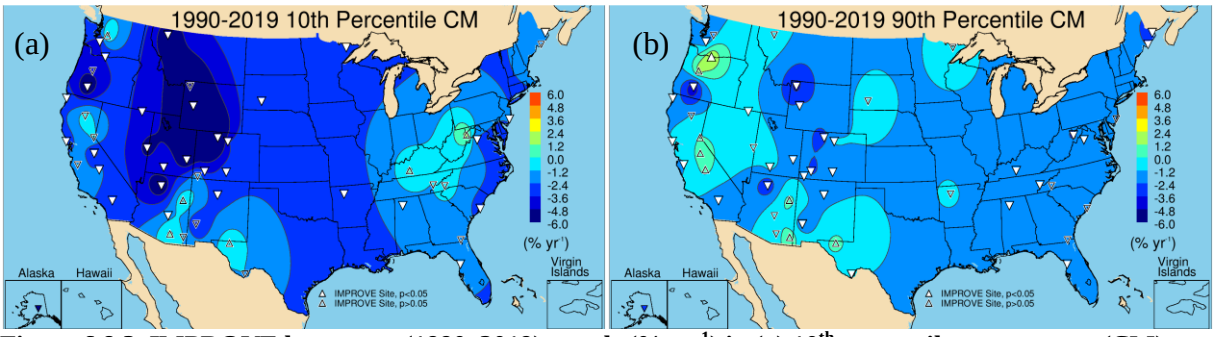

Figure 6.8.3. IMPROVE long-term (1990–2019) trends (% yr^{-1}) in (a) 10th percentile coarse mass (CM) concentrations and (b) 90th percentile concentrations. Filled triangles correspond to statistically significant trends ($p \leq 0.05$).

Short-term trends in the 10th and 90th percentile CM concentrations (Figure 6.8.4a and 6.8.4b, respectively) showed more spatial variability than the long-term trends, with many more insignificant and positive trends. The 10th percentile trends had only 22 statistically significant trends out of 137 valid sites. Of the valid sites, 72 had positive although mostly insignificant trends. The strongest statistically insignificant negative trends occurred at sites in Colorado and Montana and parts of southern California and Oregon. Statistically significant positive trends occurred at several sites, with the strongest at Shining Rock WA, North Carolina (SHRO1); Dolly Sods WA, West Virginia (DOSO1); Cohutta, Georgia (COHU1); Sawtooth National Forest (NF), Idaho (SAWT1); Lassen Volcanic NP, California (LAVO1); and Bliss SP, California (BLIS1). Trends ranged from -10.37% yr^{-1} ($p = 0.025$) at Gates of the Mountains, Montana (GAMO1), to 9.08% yr^{-1}($p = 0.005$) at Shining Rock WA, North Carolina (SHRO1).

Similar spatial patterns were seen for the short-term 90th percentile trends, with sites in the central United States, California, and the Northwest and sites in the Southeast having positive but insignificant trends. Sites with strongly decreased CM included those in Colorado. Of the 137 sites, 21 were statistically significant and ranged from -4.77% yr^{-1} ($p = 0.005$) at Upper Buffalo WA, Arkansas (UPBU1), to 5.41% yr^{-1} ($p = 0.004$) at Martha's Vineyard, Massachusetts (MAVI1). Several sites had both significant positive 10th and 90th percentile trends, such as Shining Rock WA, North Carolina (SHRO1); Cohutta, Georgia (COHU1); and Bliss SP, California (BLIS1). The short-term 10th and 90th percentiles trend maps did not reflect the corresponding FD trend maps, with the CM trends having much larger spatial variability, more insignificant trends, and fewer sites with negative trends.

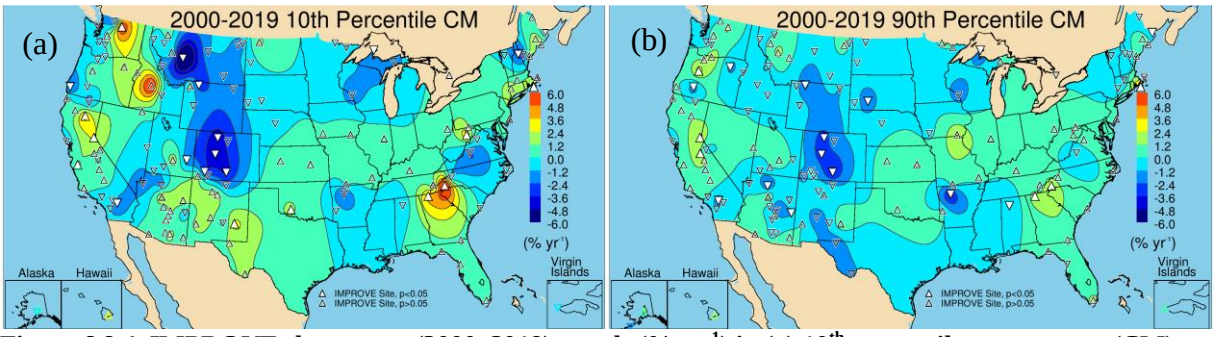

Figure 6.8.4. IMPROVE short-term (2000–2019) trends (% yr^{-1}) in (a) 10th percentile coarse mass (CM) concentrations and (b) 90th percentile concentrations. Filled triangles correspond to statistically significant trends ($p \leq 0.05$).

Comparisons of short-term regional mean percentile CM trends are shown in Figure 6.8.5. Unlike the results for FD trends (Figure 6.5.5), most of the regional mean trends were statistically insignificant, except for the positive 50th percentile trend in the Northeast region. The Central region had positive trends for all percentiles, although insignificant, while the Midsouth had negative trends, also insignificant. The California region had insignificant but weakly positive trends. CM trends were notable because they indicate that CM has not decreased across large regions of the United States, unlike FM.

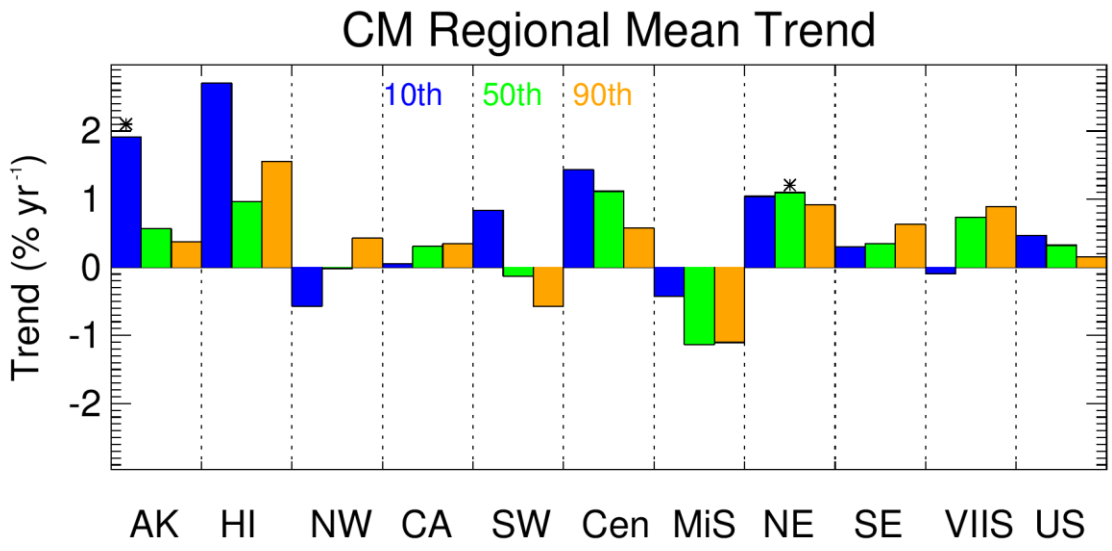

Figure 6.8.5. Short-term (2000–2019) regional mean trends (% yr^{-1}) in 10th, 50th, and 90th percentile coarse mass (CM) concentrations. Regions are arranged from western to eastern United States (AK = Alaska, HI = Hawaii, NW = Northwest, CA= California, SW = Southwest, Cen = Central, MiS = Midsouth, NE = Northeast, SE = Southeast, VIIS = Virgin Islands, and US = all sites). Statistically significant trends ($p \leq 0.05$) are denoted with "*".

6.9 f_{abs} TRENDS

Recalibration of f_{abs} began in 2003 (White et al., 2016); therefore, only short-term trends were computed. Trends in f_{abs} could be influenced by changes in absorbing aerosol due to both

EC and/or FD. The short-term annual mean f_{abs} trend is shown in Figure 6.9.1. Of the 127 valid sites, 59 were statistically significant and ranged from -4.72% yr^{-1} ($p < 0.001$) at San Gorgonio WA, California (SAGO1), to 3.99% yr^{-1} ($p = 0.024$) at Lostwood, North Dakota (LOST1). Several sites in North Dakota and Montana were associated with positive f_{abs} trends, likely associated with oil and gas development (Gebhart et al., 2018). EC trends were insignificant in this same region. Trends at sites across the northwestern United States were also largely insignificant and many were positive, likely due to biomass smoke impacts. Trends were also insignificant and positive at sites across parts of the southwestern United States, such as New Mexico and Colorado. These regions also experienced positive and insignificant FD trends.

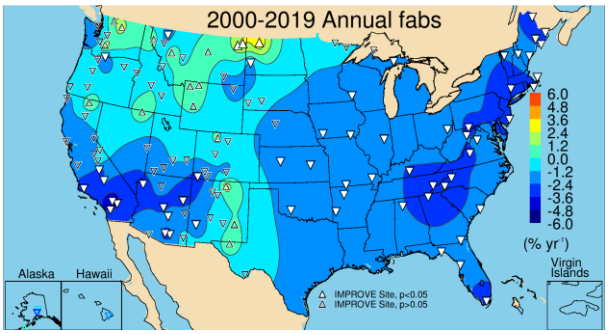

Figure 6.9.1. Annual mean filter absorption (f_{abs}) short-term (2000–2019) trends (% yr^{-1}). Filled triangles correspond to statistically significant trends ($p \leq 0.05$).

Comparisons of regional seasonal mean short-term trends are shown in Figure 6.9.2. Statistically significant reductions in seasonal mean f_{abs} occurred at most regions but especially in the eastern United States. The Northeast, Southeast, and Midsouth regions all experienced similar reductions across all seasons (-2% yr^{-1} to -3% yr^{-1}). In comparison, EC trends in the same regions were stronger during summer relative to other seasons. Weaker reductions in f_{abs} occurred in the Central and Southwest regions, with some seasonal trends that were insignificant, especially during summer. In the California region, strong reductions in f_{abs} occurred in spring and fall, while negative but insignificant trends occurred during winter and summer. The Northwest region had no statistically significant trends; most seasons were negative except for summer, which was weakly positive and likely influenced by biomass smoke. Seasonal mean trends in the Hawaii, Alaska, and Virgin Islands regions were mostly insignificant.

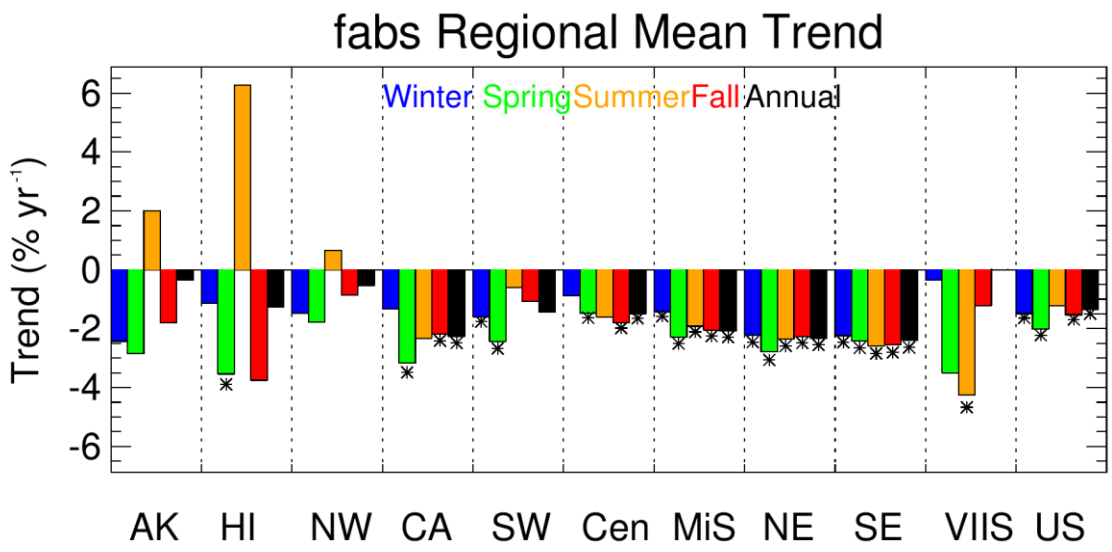

Figure 6.9.2. Short-term (2000–2019) regional seasonal mean filter absorption (f_{abs}) trends (% yr^{-1}) for major U.S. regions for winter, spring, summer, fall, and annual means. Regions are arranged from western to eastern United States (AK = Alaska, HI = Hawaii, NW = Northwest, CA= California, SW = Southwest, Cen = Central, MiS = Midsouth, NE = Northeast, SE = Southeast, VIIS = Virgin Islands, and US = all sites). Statistically significant trends ($p \leq 0.05$) are denoted with "*".

Short-term trends in the 10th percentile f_{abs} showed strong reductions at sites in the eastern United States, where most sites had statistically significant trends, except in the northeastern United States (Figure 6.9.3a). Of the 132 valid sites, 45 sites had statistically significant trends, most in the eastern United States. Trends ranged from -16.92% yr^{-1} ($p = 0.028$) in Mount Hood, Oregon (MOHO1), to 3.77% yr^{-1} ($p = 0.022$) at Lostwood, North Dakota (LOST1). Many of the 10th percentile trends could be affected by normalization by very low f_{abs} median values. The spatial patterns are different from those observed in the 10th percentile EC trends.

The 90th percentile f_{abs} trends (Figure 6.9.3b) showed similar spatial patterns as the 10th percentile trends. Strong reductions in f_{abs} at sites across the eastern United States were statistically significant, while reductions at sites in the West were much weaker, positive, and insignificant. However, sites in southern California, Arizona, and parts of Oregon also experienced strong reductions. Many of the insignificant and positive trends at sites in the northwestern and southwestern United States were similar to EC and FD trends, respectively, and these likely influenced the f_{abs} trends. The 90th percentile trends ranged from -4.48% yr^{-1} ($p < 0.001$) at San Gorgonio WA, California (SAGO1), to 3.03% yr^{-1} ($p = 0.017$) at Medicine Lake, Montana (MELA1).

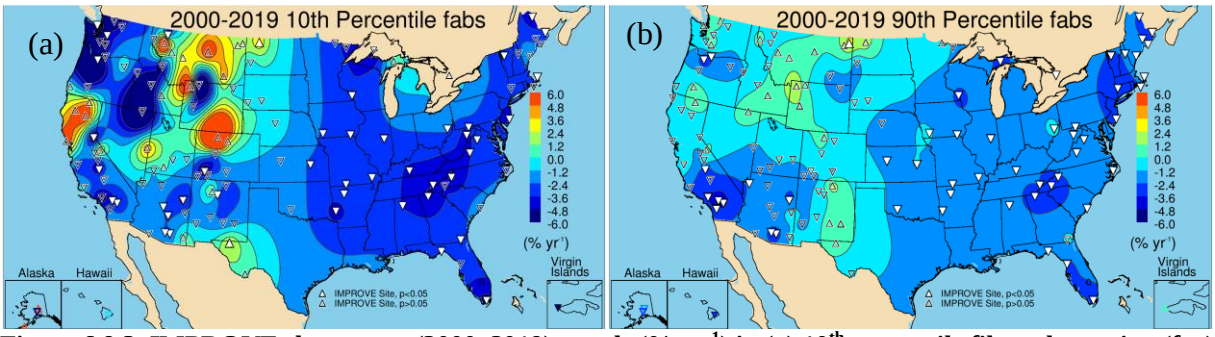

Figure 6.9.3. IMPROVE short-term (2000–2019) trends (% yr^{-1}) in (a) 10th percentile filter absorption (f_{abs}) and (b) 90th percentile f_{abs}. Filled triangles correspond to statistically significant trends ($p \leq 0.05$).

Regional mean percentile trends are shown in Figure 6.9.4. The Northeast, Southeast, and Central regions had statistically significant trends, with somewhat higher reductions for the 10th percentile f_{abs}, which may be an artifact of normalization by very low f_{abs} values. In the Southwest region, the 50th percentile had significant reductions in f_{abs}, but the 90th percentile trend was weak and insignificant. This was the general pattern for the Northwest and California regions, where the 90th percentile f_{abs} trends were negative but insignificant.

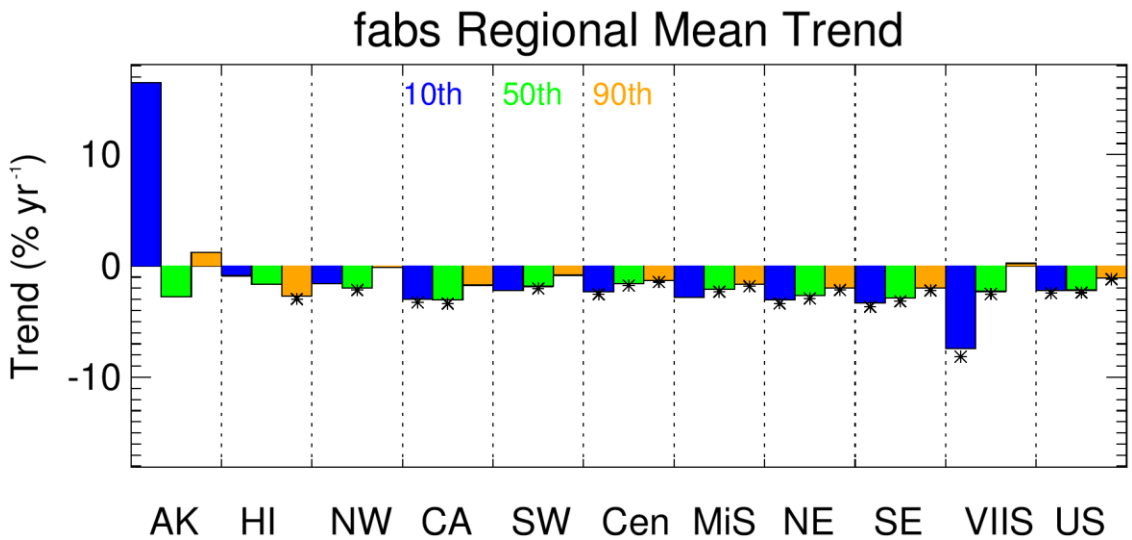

Figure 6.9.4. Short-term (2000–2019) regional mean trends (% yr^{-1}) in 10th, 50th, and 90th percentile filter absorption (f_{abs}). Regions are arranged from western to eastern United States (AK = Alaska, HI = Hawaii, NW = Northwest, CA= California, SW = Southwest, Cen = Central, MiS = Midsouth, NE = Northeast, SE = Southeast, VIIS = Virgin Islands, and US = all sites). Statistically significant trends ($p \leq 0.05$) are denoted with "*".

6.10 DISCUSSION

Timelines of regional, annual mean mass concentrations for $PM_{2.5}$ sulfate ion, nitrate ion, OC, EC, and FD that correspond to previous trend results are shown in Figure 6.10.1(a-j) for 2001 through 2019. Regional mean concentrations for 2000 were not included due to the expansion of the network in that year (Hand et al., 2020). Similar timelines for CM

concentrations are shown in Figure 6.10.2(a-j). These mass concentrations do not include mass correction factors for sulfate, nitrate, or OC (e.g., concentrations are for sulfate ion, not ammonium sulfate); therefore, the sum of individual bars should not be interpreted as RCFM, such as is shown in Chapter 3. However, the basic patterns are similar and reflect both RCFM and FM. It is clear from these timelines and the previous trend discussions that strong reductions in FM have occurred at nearly all remote regions across the United States. These reductions were greatest in the East and driven by strong negative trends in sulfate ion concentrations. Sulfate concentrations have decreased in response to dramatic reductions in sulfur dioxide emissions due to regulatory activity (Hand et al., 2020). In addition, reductions in nitrate ion and OC concentrations (especially in the East) have contributed to reduced FM. Negative trends in nitrate concentrations at sites in southern California occurred at sites where nitrogen dioxide emissions, especially mobile emissions, have declined due to regulatory activity.

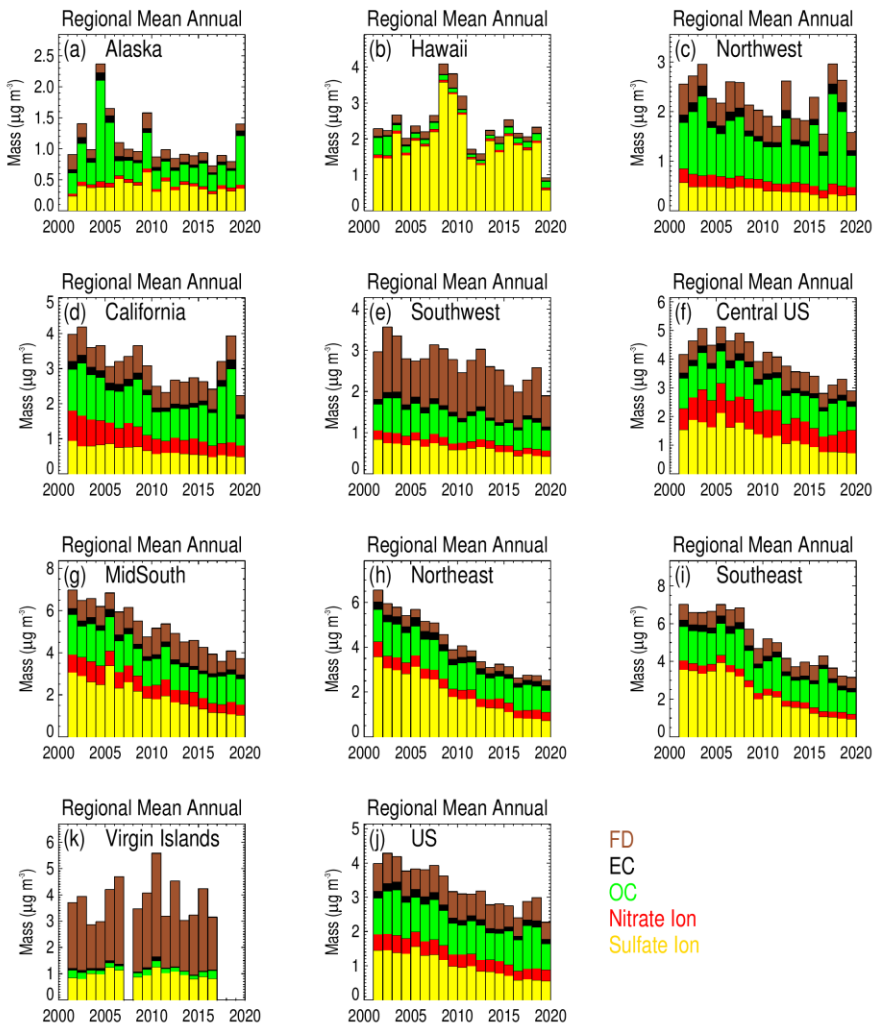

Figure 6.10.1. Short-term (2001–2019) timelines in IMPROVE regional, annual mean mass concentrations (µg m^{-3}) for sulfate ion, nitrate ion, organic carbon (OC), elemental carbon (EC), and fine dust (FD).

At sites in the western United States, especially the Northwest, FM has declined at a weaker rate relative to sites in the East. Comparisons of OC and EC trends suggest that FM is influenced by an increase in biomass burning impacts that have led to an increase in OC, or at the very least flat and insignificant trends. Hire fire years are especially evident for 2017 and 2018 in Figure 6.10.1.c. OC is a major contributor to FM, especially at western sites, and has influenced FM trends in the region (McClure and Jaffe, 2018).

FM concentrations at sites in the Southwest have decreased (many insignificantly), although to a lower extent relative to sites in the East. The FM budget at these sites includes a significant fraction of FD, and trends in FD were insignificant (Figure 6.10.1e). OC trends were also insignificant at many southwestern sites, suggesting that the role of FD and OC may have influenced FM trends in the region.

PM_{10} trends were spatially similar to FM trends at sites in the East, where CM concentrations were relatively low, and therefore declines in sulfate and OC concentrations also led to reductions in PM_{10}. However, FM and PM_{10} trends at sites in the West were different, mainly at sites in the central and southwestern United States. Sites in these regions have a large contribution from CM (Figure 6.10.2). CM trends were notably different from $PM_{2.5}$ speciated trends in that only a few sites across the United States had statistically significant negative CM trends. Several sites had statistically significant positive trends. These CM trends appeared to affect the PM_{10} trends at those sites.

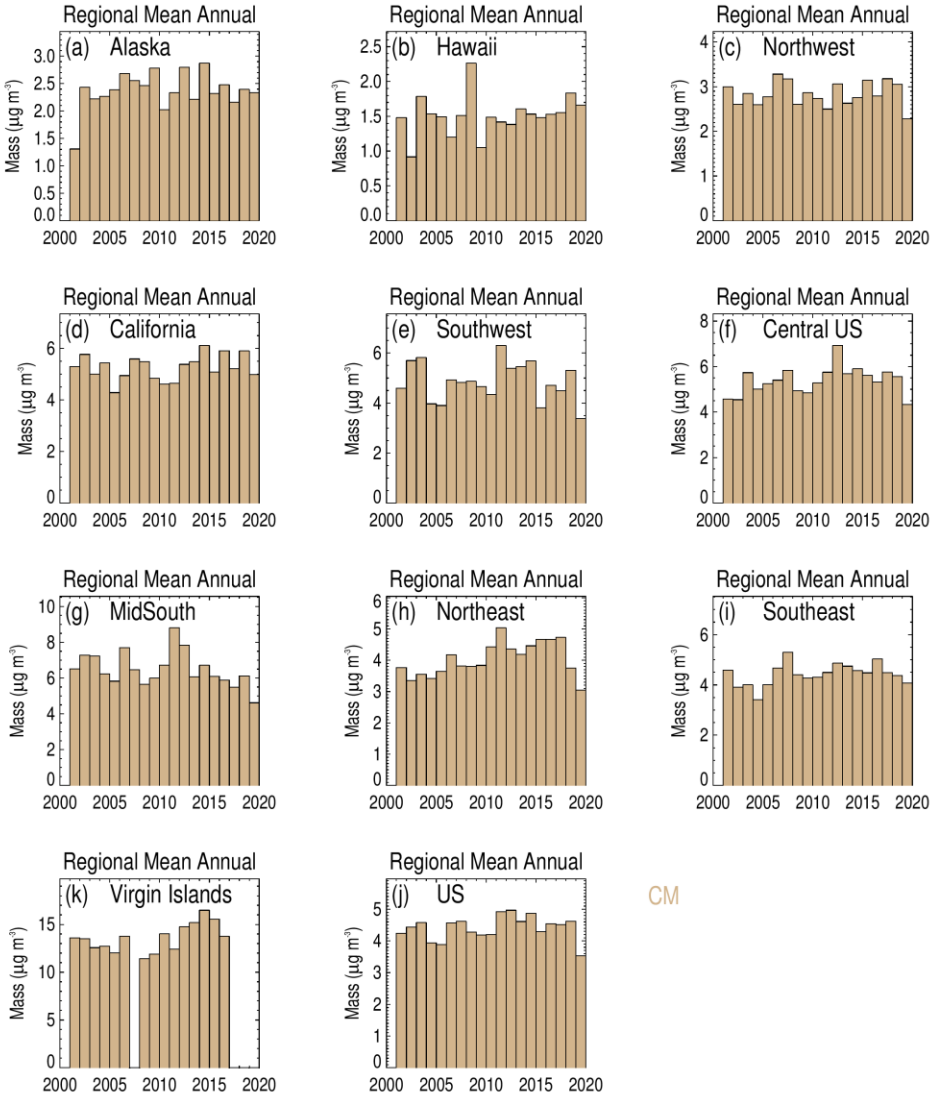

Figure 6.10.2. Short-term (2001–2019) timelines in IMPROVE regional, annual mean coarse mass (CM) concentrations (µg m^{-3}).

Regulatory activity has been very successful at reducing pollutant emissions that lead to secondary aerosols, such as sulfate, nitrate, and OC, as well as reductions in primary aerosols such as EC, and some OC, depending on its sources. Reductions in these species have driven negative trends in FM and PM_{10} at sites across the United States. However, the role of natural aerosols, such as those derived from biomass smoke and dust storms have not declined and for some sites and seasons have increased. The impact of these positive trends have and likely will continue to impede progress in reducing FM and PM_{10} concentrations.

Site-specific long-term and short-term annual mean trend results are provided in Appendix 6.1, short-term percentile trends in Appendix 6.2, and long-term percentile trends in Appendix 6.3.

REFERENCES

Blanchard, C., Hidy, G., Shaw, S., Baumann, K., and Edgerton, E. (2016), Effects of emission reductions on organic aerosol in the southeastern United States, *Atmospheric Chemistry and Physics*, *16*(1), 215-238, doi:10.5194/acp-16-215-2016.

Chow, J. C., Watson, J. G., Chen, L.-W. A., Chang, M. O., Robinson, N. F., Trimble, D., and Kohl, S. (2007), The IMPROVE_A temperature protocol for thermal/optical carbon analysis: maintaining consistency with a long-term database, *Journal of the Air & Waste Management Association*, *57*(9), 1014-1023, https://doi.org/10.3155/1047-3289.57.9.1014.

Debell, L. J. (2006), Data Validation Historical Report No 3, http://vista.cira.colostate.edu/improve/wp-content/uploads/2022/09/044_Historical_QA_Report_Nitrate.pdf.

Evanoski-Cole, A., Gebhart, K., Sive, B., Zhou, Y., Capps, S., Day, D., Prenni, A., Schurman, M., Sullivan, A., and Li, Y. (2017), Composition and sources of winter haze in the Bakken oil and gas extraction region, *Atmospheric Environment*, *156*, 77-87, http://dx.doi.org/10.1016/j.atmosenv.2017.02.019.

Feng, J., Chan, E., and Vet, R. (2020), Air quality in the eastern United States and eastern Canada for 1990–2015: 25 years of change in response to emission reductions of SO2 and NOx in the region, *Atmospheric Chemistry and Physics*, *20*(5), 3107-3134, doi:10.5194/acp-20-3107-2020.

Gebhart, K. A., Day, D. E., Prenni, A. J., Schichtel, B. A., Hand, J. L., and Evanoski-Cole, A. R. (2018), Visibility impacts at Class I areas near the Bakken oil and gas development, *Journal of the Air & Waste Management Association*, *68*(5), 477-493, doi:10.1080/10962247.2018.1429334.

Hand, J. L., Schichtel, B. A., Malm, W. C., and Pitchford, M. L. (2012), Particulate sulfate ion concentration and SO2 emission trends in the United States from the early 1990s through 2010, *Atmospheric Chemistry and Physics*, *12*(21), 10353-10365, doi:10.5194/acp-12-10353-2012.

Hand, J. L., Prenni, A. J., Schichtel, B. A., Malm, W. C., and Chow, J. C. (2019), Trends in remote PM2.5 residual mass across the United States: Implications for aerosol mass reconstruction in the IMPROVE network, *Atmospheric Environment*, *203*, 141-152, doi:10.1016/j.atmosenv.2019.01.049.

Hand, J. L., Prenni, A. J., Copeland, S., Schichtel, B. A., and Malm, W. C. (2020), Thirty years of the Clean Air Act Amendments: Impacts on haze in remote regions of the United States (1990–2018), *Atmospheric Environment*, *243*, 117865, https://doi.org/10.1016/j.atmosenv.2020.117865.

Hyslop, N. P., Trzepla, K., and White, W. H. (2015), Assessing the suitability of historical PM2. 5 element measurements for trend analysis, *Environmental Science & Technology*, *49*(15), 9247-9255, doi:10.1021/acs.est.5b01572.

Isaaks, E. H., and Mohan Srivastava, R. (1989), *An Introduction to Applied Geostatistics*, Oxford University Press, New York, ISBN 978-0195050134.

Kharol, S. K., McLinden, C. A., Sioris, C. E., Shephard, M. W., Fioletov, V., van Donkelaar, A., Philip, S., and Martin, R. V. (2017), OMI satellite observations of decadal changes in ground-level sulfur dioxide over North America, *Atmospheric Chemistry and Physics*, *17*(9), 5921-5929, doi:10.5194/acp-17-5921-2017.

Krotkov, N. A., McLinden, C. A., Li, C., Lamsal, L. N., Celarier, E. A., Marchenko, S. V., Swartz, W. H., Bucsela, E. J., Joiner, J., Duncan, B. N., Boersma, K. F., Veefkind, J. P., Levelt, P. F., Fioletov, V. E., Dickerson, R. R., He, H., Lu, Z., and Streets, D. G. (2016), Aura OMI observations of regional SO2 and NO2 pollution changes from 2005 to 2015, *Atmos. Chem. Phys.*, *16*(7), 4605-4629, doi:10.5194/acp-16-4605-2016.

Malm, W. C., Schichtel, B. A., Hand, J. L., and Collett Jr, J. L. (2017), Concurrent temporal and spatial trends in sulfate and organic mass concentrations measured in the IMPROVE monitoring program, *Journal of Geophysical Research: Atmospheres*, *122*, 10462-10476, doi:10.1002/2017JD026865.

Malm, W., Schichtel, B., Hand, J., and Prenni, A. (2020), Implications of organic mass to carbon ratios increasing over time in the rural United States, *Journal of Geophysical Research: Atmospheres*, *125*(5), e2019JD031480, doi:10.1029/2019JD031480.

McClure, C. D., and Jaffe, D. A. (2018), US particulate matter air quality improves except in wildfire-prone areas, *Proceedings of the National Academy of Sciences*, *115*(31), 7901-7906, doi:doi:10.1073/pnas.1804353115.

McDade, C. (2004), Summary of IMPROVE nitrate measurements, http://vista.cira.colostate.edu/improve/Publications/GrayLit/025_IMPROVEnitrate/Nitrate%20Summary_1004.pdf.

McDade, C. (2007), Diminished wintertime nitrate concentrations in late 1990s, *IMPROVE Data Advisory*, http://vista.cira.colostate.edu/improve/Data/QA_QC/Advisory/da0002/da0002_WinterNO3.pdf.

Prenni, A., Day, D., Evanoski-Cole, A., Sive, B., Hecobian, A., Zhou, Y., Gebhart, K., Hand, J., Sullivan, A., and Li, Y. (2016), Oil and gas impacts on air quality in federal lands in the Bakken region: An overview of the Bakken Air Quality Study and first results, *Atmospheric Chemistry and Physics*, *16*(3), 1401-1416, doi:10.5194/acp-16-1401-2016.

Schichtel, B. A. (2003), Underestimation of sulfur concentrations during high loadings and humidity conditions in the eastern US, *IMPROVE Data Advisory*, http://vista.cira.colostate.edu/improve/Data/QA_QC/Advisory/da0001/da0001_S_underestimation.htm.

Schichtel, B. A., Malm, W. C., Beaver, M., Copeland, S., Hand, J. L., Prenni, A. J., Rice, J., and Vimont, J. (2021), The future of carbonaceous aerosol measurement in the IMPROVE monitoring program, http://vista.cira.colostate.edu/improve/wp-content/uploads/2021/10/041_CarbonReport_Final.pdf.

Theil, H. (1950), A rank-invariant method of linear and polynomial regression analysis., *Proc. Kon. Ned. Akad. v Wetensch.*, *A*(53), 386-392, https://doi.org/10.1007/978094-011-2546-8_20.

White, W. H. (2006), Elemental concentrations above the MDL can go undetected, *IMPROVE Data Advisory* (da0010), http://vista.cira.colostate.edu/improve/Data/QA_QC/Advisory/da0010/da0010_Almdl.pdf.

White, W. H. (2007), Shift in EC/OC split with 1 January 2005 TOR hardware upgrade, *IMPROVE Data Advisory* (da0016), http://vista.cira.colostate.edu/improve/Data/QA_QC/Advisory/da0016/da0016_TOR2005.pdf.

White, W. H. (2015), Changed reporting of light absorption, *IMPROVE Data Advisory* (da0033), http://vista.cira.colostate.edu/improve/Data/QA_QC/Advisory/da0033/da0033_Fabs.pdf.

White, W. H. (2016), Increased variation of humidity in the weighing laboratory, *IMPROVE Data Advisory* (da0035), http://vista.cira.colostate.edu/improve/Data/QA_QC/Advisory/da0035/da0035_IncreasedRH.pdf.

White, W. H., Trzepla, K., Hyslop, N. P., and Schichtel, B. A. (2016), A critical review of filter transmittance measurements for aerosol light absorption, and de novo calibration for a decade of monitoring on PTFE membranes, *Aerosol Science and Technology*, *50*(9), 984-1002, http://dx.doi.org/10.1080/02786826.2016.1211615.

Zhang, X. (2019), Correction of chloride concentrations for filter blank levels, *IMPROVE Data Advisory* (da0039), http://vista.cira.colostate.edu/improve/Data/QA_QC/Advisory/da0039/da0039_ChlorideOverCorrection.pdf.